Integrated multi-omics analysis uncovers roles of mdm-miR164b-*MdORE1* in strigolactone mediated inhibition of adventitious root formation in apple

Xingqiang Fan[1], Hui Li[1], Yushuang Guo[1], Qi Qi[1,2], Xiangning Jiang[2], Yi Wang[1], Xuefeng Xu[1], Changpeng Qiu[1], Wei Li[1]*, Zhenhai Han[1]*

[1]State Key Laboratory of Agrobiotechnology, College of Horticulture, China Agricultural University, Beijing 100193, China
[2]National Engineering Laboratory for Tree Breeding, College of Life Sciences and Biotechnology, Beijing Forestry University, Beijing 100083, China

*Authors to whom correspondence should be addressed.
Corresponding authors contact information:
Zhenhai Han: rschan@cau.edu.cn; Wei Li: liwei0522898@163.com

Author Contributions

Z.H. and W.L. conceived and designed the experiments; X.F., H.L. and Y.G. performed the experiments; Q.Q and X.J. was responsible for endogenous hormone analyses; Y.W., X.X., and C.Q. provided suggestions on experiments and manuscript editing; Z.H., W.L., and X.F. wrote and edited the manuscript. All authors read and approved the manuscript.

Conflict of interest

The authors declare no conflict of interest.

Total word count: 7,040
Introduction: 943
Materials and Metheds: 1,853
Result: 3,050
Discussion: 1,138
Acknowledgements: 73
Number of figures: 8, all of the figures should be in color
Number of tables: 1
Number of supporting information: Supplemental figures: 10

Supplemental figures：5

Summary

Adventitious root (AR) formation is important for the vegetative propagation. The effects of strigolactones (SLs) on AR formation have been rarely reported, especially in woody plants. In this study, we first verified the inhibitory effects of SLs on AR formation in apple materials. Transcriptome analysis identified 12,051 differentially expressed genes over the course of AR formation, with functions related to organogenesis, cell wall biogenesis or plant senescence. WGCNA suggests SLs might inhibit AR formation through repressing the expression of two core hub genes, *MdLAC3* and *MdORE1*. We further verified that enhanced cell wall formation and accelerated senescence were involved in the AR inhibition caused by SLs. Combining small RNA and degradome sequencing, as well as a dual-luciferase sensor system, we identified and validated three negatively correlated miRNA–mRNA pairs, including mdm-miR397–*MdLAC3* involved in secondary cell wall formation, and mdm-miR164a/b–*MdORE1* involved in senescence. Finally, we have experimentally demonstrated the role of mdm-miR164b–*MdORE1* in SLs-mediated inhibition of AR formation. Overall, our findings not only propose a comprehensive regulatory network for the function of SLs on AR formation, but also provide novel candidate genes for the potential genetic improvement of AR formation in woody plants using transgenic or CRISPR technology.

Keywords: Apple; Strigolactones; Adventitious Root; Root Primordia; Cell Wall; Senescence

Introduction

Vegetative propagation is important for keeping the desirable gene combinations of a superior cultivar (Kang, Li, Liyuan, & Hao, 2019). Vegetative propagation methods have been widely used in the horticultural industry because most horticultural crops are heterozygous, and beneficial traits are difficult to be maintained by sexual reproduction (Amano et al., 2020). Cutting propagation is one of the most efficient and economical methods of vegetative propagation to produce large numbers of clonal offspring from a plant with desirable traits in a short period of time (Z. Wang et al., 2019). Adventitious root (AR) formation is a prerequisite for the success of propagation via cuttings. However, it is difficult to induce ARs in many plant species, which largely limits the development and scale of many horticulture industries (K. Li et al., 2019).

The formation of ARs during cutting propagation can be divided into four stages, based on physiological and metabolic markers. In stage 1, cells are activated by internal and external factors and in stage 2, cell division promotes the formation of AR primordia. Stage 3 is characterized by the formation of AR primordia and stage 4 represents AR emergence (Atkinson et al., 2014; Klerk, B, R, & KH, 1997; Legué, Rigald, & Bhaleraod, 2014). However, ARs may originate from different tissues in different species; for instance, in herbaceous species such as *Arabidopsis thaliana*, AR primordia originate from cells in the stem pericycle (Della Rovere et al., 2013), whereas in woody species such as poplar, they form at the phloem/cambium junction of stems (Rigal et al., 2012). Therefore, the rooting mechanism of woody plants can be distinct from that of herbaceous plants (Abarca, Pizarro, Amo, & Diaz-Sala, 2011; Birnbaum & Sanchez Alvarado, 2008; Ludwig-Muller, Vertocnik, & Town, 2005).

Several plant hormones have been implicated in AR formation (da Costa et al., 2013; Della Rovere et al., 2013; Mehrotra et al., 2014; Muday, Rahman, & Binder, 2012). Among these, auxin is one of the most well-studied hormones and promotes both AR and lateral root formation (Negi, Sukumar, Liu, Cohen, & Muday, 2010; Zhao et al., 2001). In the early 1930s, indole-3-acetic acid (IAA) was shown to effectively induce

AR formation (X. Xu et al., 2017) and its synthetic analog indole-3-butyric acid (IBA) has been widely used to induce ARs in woody plants. Several studies have analyzed the molecular mechanisms of auxin-mediated AR formation and have reported that auxin response factors (ARFs), such as *ARF6* and *ARF8*, are positive regulators of adventitious rooting, whereas *ARF17* negatively regulates AR formation (Bellini, Pacurar, & Perrone, 2014; Gutierrez et al., 2012). Additionally, ARF proteins regulate AR formation by regulating the expression of *LATERAL ORGAN BOUNDARIES DOMAIN PROTEIN* (*LBD*) genes by binding to their promoters (Majer, Xu, Berendzen, & Hochholdinger, 2012; Okushima, Fukaki, Onoda, Theologis, & Tasaka, 2007).

Strigolactones (SLs) comprise a recently reported class of hormones that function as plant signaling molecules for soil organisms (Gamir et al., 2020; Lopez-Raez, Shirasu, & Foo, 2017). The functions of SLs associated with shoot and root development have also been studied, and SLs repress shoot branching in Arabidopsis, rice, petunia, and pea (Brewer, Koltai, & Beveridge, 2013; Gomez-Roldan et al., 2008; Umehara et al., 2008). The mechanisms of SL-mediated shoot branching had been relatively well characterized: for instance, in the regulation of rice tillering, SLs induce the expression of *CYTOKININ OXIDASE/DEHYDROGENASE 9* (*OsCKX9*), which encoding proteins to catalyze the degradation of endogenous cytokinins (Duan et al., 2019). Recently, SLs also have been shown to inhibit AR formation during vegetative propagation. In Arabidopsis, treatment with the exogenous synthetic SL analog GR24 significantly suppressed AR formation. Conversely, a SL-signaling mutant, *more axillary growth 2* (*max2*), produced more ARs than wild type (Rasmussen et al., 2012). Similarly, in tomato, knock-down of *CAROTENOID CLEAVAGE DIOXYGENASE 8*, a key SLs biosynthesis gene, led to an 89% increase in the number of ARs during cutting propagation (Kohlen et al., 2012). Although a function for SLs in AR formation has been reported for several species, the molecular mechanism involved is less well known. Furthermore, most of reports about SLs-mediated AR formation focus on herbaceous plants, such as Arabidopsis, petunia, and tomato, and the function of SLs in AR formation of woody plants has rarely been addressed.

MicroRNAs (miRNAs) comprise a class of small single-stranded noncoding RNAs that are encoded by endogenous genes. Plant miRNAs repress translation at the post-transcriptional level and play key roles in many processes, including root growth and patterning, floral organ identity and lignin synthesis (Damodharan, Corem, Gupta, & Arazi, 2018; Shanfa Lua, Jingyuan Songa, & Chiangb, 2013; L. Zheng et al., 2019). Several miRNAs associated with auxin signal transduction have been demonstrated to control AR formation (You et al., 2014). In Arabidopsis, for example, miR167 negatively regulates AR formation by targeting *ARF6* and *ARF8*, whereas miR160, targeting *ARF17*, positively regulates AR formation (Gutierrez et al., 2009; S. Liu et al., 2020). In poplar softwood cuttings, a miR167a–*PeARF8.1* module plays a crucial role in regulating AR formation (Cai et al., 2019). Although these miRNAs have been shown to have important functions in auxin-mediated AR formation, their regulatory mechanisms are elusive and more miRNAs remain to be identified.

To characterize the effects of SLs on AR formation in woody plants, as well as to understand their molecular function, we sequenced the transcriptome, small RNAs and the degradome of 30 samples from three treatments (untreated control, or treated with GR24 or IBA) at four timepoints (0, 1, 3, or 7 days after rooting). We identified differentially expressed genes (DEGs), as well as miRNAs and their targets, that are associated with AR formation. We also propose a network that delineates the interactions among the involved regulation pathways.

Materials and Methods

Evaluation of AR formation with different treatments

Five *Malus* materials, including Royal Gala, GL-3, M26, *Malus xiaojinensis*, and *Malus baccata* were used. The stem cuttings of Royal Gala and M26 were first cultured in 1/2MS (Murashige and Skoog) medium that contained a concentration series of 0, 1.25, 2.5, 5, 10, 20 μM GR24. Then, apple stem cuttings from all five genotypes were cultured in four different rooting media, including 1/2MS + ddH_2O, 1/2MS + IBA (0.3 mg L^{-1}), 1/2MS + GR24 (10 μM), or 1/2MS + IBA (0.3 mg L^{-1}) + GR24 (10 μM). The

rooting rate (AR number/number of cuttings ×100%), AR number, and AR length were recorded two weeks after rooting for each treatment. *Arabidopsis thaliana* wild type (Col-0) and *max3-4* homozygous mutants were germinated on plates containing 1/2MS medium after surface sterilization in 75% ethanol for 30 s, then in 30% bleach + 0.1% Triton X-100 for 20 min (Rasmussen et al., 2012). The plates were placed in the dark at 4°C for 3 days and then transferred to the light at 21°C with a 16-h light/8-h dark cycle. Seedlings that produced four leaves were placed in the dark again for another 4 days to elongate, and then the seedlings were moved to 16-h light/8-h dark. After 3 days, seedlings showing uniform growth were selected for cutting root segments and the remaining hypocotyl material was placed in 1/2MS medium with GR24 (5 μM) treatment or no treatment. The rooting rate for each treatment was recorded. Tobacco plants were grown at 23-24°C with a 16-h light/8-h dark cycle.

Transcriptome sequencing and data analysis

For transcriptome analysis, 0.5-cm sections from the base of apple stem cuttings from the control, 10 μM GR24, or 0.3 mg L^{-1} IBA treatments were harvested at 0, 1, 3, or 7 days after rooting with three biological replicates for each. In total, 30 libraries were generated following the manufacturer's recommendations (Zhong Wang, Gerstein, & Snyder, 2009). The qualified libraries were sequenced on illumina NovaSeq 6000. Clean data were obtained by using the FastQC tool. Differentially expressed genes were identified using the R package DEseq as previously described (Anders & Huber, 2010). The k-means script and WGCNA package in R were used. The data were processed using MapMan (version 3.6.0RC1) and GraphPad Prism8. The sequencing data have been uploaded to NCBI Sequence Read Archive with the bioproject ID PRJNA650149.

Quantification of endogenous hormone levels

Apple stem cuttings from the control or 10 μM GR24 treatments were collected at 0, 1, 3 or 7 days after rooting for hormone analysis. Fresh samples were weighed and immediately frozen in liquid nitrogen. The hormone measurements were performed by HPLC-ESI-MSn (high performance liquid chromatography coupled with electrospray

ionization multi-tandem mass spectrometry) at Beijing Forestry University (W. Chen, Gai, Liu, Wang, & Jiang, 2010; Shichang Liu, Chen, Qu, Gai, & Jiang, 2013). The endogenous hormone levels were presented as the means of three biological replicates. The hormone levels of each comparison were subjected to two-tailed Student's t-test with pooled variance.

Measurement of chlorophyll content

The content of chlorophyll was measured by using the ways previously described with minor modifications (An et al., 2019). In brief, apple leaves were cut into little pieces and immersed in 95% ethanol at room temperature in dark until completely decolorized. The absorbance was measured by a spectrophotometer at 649 nm and 665 nm.

Paraffin embedding and histological analysis

Apple stem cuttings without treatment, with 10 μM GR24 treatment, or with 0.3 mg L^{-1} IBA treatment were collected 0, 1, 3, or 7 days after rooting and embedded in paraffin according to the protocol of (X. Xu et al., 2017), with minor modifications. A 0.5-cm section from the base of each cutting was selected and fixed in FAA (formaldehyde/ethanol/acetic acid) solution. After a series of standard procedures, including dehydration, 10 μm-thick transverse sections were sectioned with a rotatory microtome (KD-2258, KEDEE, China) and stained with safranin/fast green. The sections were examined under a light microscope.

Transmission electron microscopy (TEM) for secondary cell wall

The apple stem cuttings from the control, 10 μM GR24, or 0.3 mg L^{-1} IBA treatments for 7 days were collected for secondary cell wall analysis. The samples were prepared according to (D. Song, Shen, & Li, 2010), with minor modifications. In brief, 2-mm-long stem bases were cut and fixed in PBS with 3% paraformaldehyde and 0.5% glutaraldehyde (0.1 M, pH 7.4), and were stored at 4℃ overnight. After a series washing, fixation, dehydration and embedding steps, these paraffin-embedded stems were then cut into ultrathin sections (60–80 nm) and were stained with 2% uranyl

acetate and lead citrate. The sections were examined with a TEM (Hitachi HT7700 electron microscope).

Scanning electron microscopy

The hypocotyl material from *A. thaliana* WT and *max3* (*max3-4*) in 1/2MS medium with or without 10 μM GR24 for five days was fixed in 2.5% glutaraldehyde at 4°C for 24 h. Subsequently, the samples were washed with PBS (pH 7.2) three times, and fixed in 1% (v/v) OsO_4. Then, the fixed samples were dehydrated with a gradient of six ethanol concentrations (30, 50, 70, 80, 90, and 100%). After drying, the samples were sputter-coated with 10-μm-thick gold. Images were taken with a scanning electron microscope (Regulus8100, Hitachi).

Lignin staining

To visualize lignin distribution, the hypocotyl segments of *A. thaliana* WT and *max3* (*max3-4*) treated with 10 μM GR24 or the untreated controls, were analyzed. The base of the hypocotyls was collected and fixed in FAA solution and 20–25-μm thick sections were placed on glass slides. Then, 50–100 μL lignin-acidizing reagent was added, followed by an equal amount of phloroglucinol-HCl staining solution (SPEE, 1987). Images were captured with a microscope.

Small RNA sequencing and data analysis

For small RNA sequencing, the same samples were collected as for transcriptome sequencing. Small RNAs were extracted and libraries were created using the TruSeq Small RNA Sample Prep Kit (Illumina, San Diego, USA) according to the manufacturer's instructions. Thirty small RNA libraries were tested via Agilent 2100 Bioanalyzer (Agilent Technologies, Santa Clara, CA) and sequenced on an Illumina HiSeq 2500. The raw reads were filtered and processed through various quality controls such as removal of adapter sequences and common RNA families (rRNA, tRNA, snRNA, snoRNA). The filtered unique reads with length of 18–25 bp from each library were mapped to miRBase22.0 to identify the known and novel miRNAs. A heatmap of

the identified differentially expressed miRNAs was constructed using the ggplot2 package in R (version 3.6.0). The secondary structure of miRNAs was analyzed on the RNAfold webserver.

Degradome sequencing and integrated analysis with transcriptome and miRNA sequencing

Three degradome libraries were created using 0.5-cm base sections of apple stem cuttings from the control, 10 μM GR24, and 0.3 mg L^{-1} IBA treatments (M. Zhang et al., 2019). The samples from four time points were pooled for each treatment. The degradome sequencing data were analyzed using the ACGT301-DGE v1.0 program (LC Sciences, Houston, TX, USA) to screen for reads that mapped to the apple database (Addo-Quaye, Miller, & Axtell, 2009). The sequencing data have been uploaded to NCBI Sequence Read Archive (SRA, http://www.ncbi.nlm.nih.gov/sra) with the bioproject ID PRJNA649060. A network was created to connect miRNAs and their corresponding targets and was visualized analysis using Cytoscape (version 3.7.1). The topGO and the TBtools software were used for Gene Ontology (GO) enrichment analysis (Alexa & Rahnenfuhrer, 2010; C. Chen et al., 2020).

Dual-luciferase system to verify microRNA targets

A dual-luciferase sensor system was used to quantitatively and visually evaluate miRNAs targeted degradation capability. The reporter vector was derived from pGreenII-0229 with modification (Q. Liu, Wang, & Axtell, 2014). In the reporter vector, fragments (including the predicted cleavage site and 200- to 250- bp upstream and downstream of the predicted cleavage site) of each candidate miRNA target genes were cloned and fused to the 3' of the *LUC* gene, respectively. The effector vectors were conducted like the construction of the overexpression vector mdm-miR164b. The monoclonal bacteria containing the report or effector vector were cultured separately at 28℃ and then collected. After resuspension, the bacteria containing report and effector vectors were mixed in a ratio of 1:9 with a final concentration of OD_{600} at 0.8 to 1.0. Leaves of four-week-old *N. benthamiana* were infiltrated with the mixture. LUC

activities were observed and quantified at third day after infiltration. Night SHADE LB 985 (Berthold) was used to observe fluorescence signal, and LUC activities were quantified using dual-luciferase assay reagents (Promega, Madison, USA), three biological replicates were carried out for each.

Tobacco transformation and transgenic plants identification

In order to verify the impact of mdm-miR164b on AR formation, we constructed a vector for overexpression of mdm-miR164b. The precursor and flanking sequence (200-bp upstream and downstream of the precursor sequence) of mdm-miR164b was fused into the plasmid of pCAMBIA1305.1 and then the constructed vector was introduced into *Agrobacterium tumefaciens* strain EHA105 for transformation. Tobacco transformation was performed as previously described (X. Zheng et al., 2007). Genomic DNA was extracted from the leaves of putative transgenic events using a Plant Genomic DNA Extraction Kit (TIRNGEN, China). The primer pair MIR164b-F (5′-CCAGGGTTATGGGGGTCTTTAG -3′) and MIR164b-R (5′-TGTGATATGTGGCGGTGGAAAT -3′) was used to amplify a 326-bp fragment from the tobacco DNA. The putative transgenic events were also verified by histochemical GUS assays. WT or mdm-miR164b putative shoots were incubated in X-Gluc solution at 37°C overnight for histochemical GUS staining. After 16 to 18 hours of staining, the samples were transferred into successive concentrations of ethanol (50%, 60%, 70%, 80%, 90%, each 2 hours, and then storage in 100%) to remove plant pigments such as chlorophyll.

Subcellular Localization

The open reading frames of *MdORE1* without termination codon was cloned from apple cDNA and inserted into the plasmid PRI101-eGFP to fuse with eGFP. Subcellular localization was carried out as previously described (Zhao et al., 2019). Leaves of four-week-old *N. benthamiana* were selected to infiltrate bacteria solution. Fluorescence images were taken with a laser scanning confocal microscopy (Olympus, FV3000 microscope) at 488 nm wavelength. The primers are listed in Table S5.

Virus-induced gene silencing (VIGS)

VIGS was carried out as previously described (J. Chen et al., 2021). In order to explore the role of *MdORE1* in AR formation, a specific fragment of *MdORE1* sequence (419 bp in length) was amplified from apple genome to construct the vector pTRV2-*MdORE1*. pTRV1, pTRV2, and pTRV2-*MdORE1* were transformed into *Agrobacterium tumefaciens* strain GV3101, respectively. Furthermore, the bacteria containing vectors were cultured separately at 28℃ in LB medium on a sharker at 200 rpm until the final absorbance A600=1.0-1.2, and collected by centrifugation at room temperature and re-suspended using the buffer included 10 mM $MgCl_2$, 200 mM acetosyringone and 10 mM MES. Before infiltrating, a mixture of *Agrobacterium tumefaciens* carrying pTRV1 and pTRV2, or with pTRV1 and pTRV2-*MdORE1* in a ratio of 1:1 (v/v) were incubated in dark at room temperature for 3-4 h. Four-week-old stem cuttings were selected for infiltrating. The infiltrated plants were washed with sterile water three times and transfered into apple rooting medium. The root phenotype of stem cuttings was recorded 30-40 days after infiltration. The primers used in this experiment are listed in Table S5.

Results

SLs inhibit AR formation in apple stem cuttings

We first tested the effects of SL on AR formation of an apple rootstock, M26, and an apple cultivar, Royal Gala. Two weeks after exogenous treatment with GR24, a synthetic analog of SL, stem cuttings of both apple materials exhibited no AR formation (Figure 1). This complete inhibition of ARs was observed for GR24 concentrations above 10 μM (Figure 1A). We further tested the inhibitory effects of GR24 on five apple genotypes, including M26, *Malus xiaojinensis*, and *Malus baccata*, Royal Gala, and GL-3 (a seedling clone of Royal Gala with a high regeneration capacity). For all five apple genotypes, 10 μM GR24 inhibited AR formation two weeks after rooting (Figure 1B). Next, we studied the potential interaction between GR24 and IBA on AR formation. When treated with 0.3 mg L^{-1} IBA, all five apple genotypes exhibited a rooting

efficiency of more than 85% and 10 μM GR24 treatment significantly inhibited the effects of IBA, with a reduction in rooting efficiency varied from 16.67% to 40% for five apple genotypes (Figure 1B). Although some stem cuttings still produced ARs in the IBA + GR24 treatment, the number of ARs was 55% to 68% lower for all genotypes than following treatment with IBA (Figure 1C). These results suggest that SLs inhibit rooting in apple materials.

Transcriptomic differentiation under SLs treatments during AR formation

To identify genes and regulatory networks associated with the inhibitory effects of SLs on AR formation, we performed a time-course RNA-seq analysis for basal sections of stem cuttings without treatment (Control, M), with 10 μM GR24 treatment (G), or with 0.3 mg L^{-1} IBA treatment (A). RNA-seq generated 41.75 to 69.42 million pair-ended reads for each sample, and a total of 1,558 billion paired-end reads for all 30 libraries (Table S1). Among all the identified 12,051 DEGs during the course of AR formation, 8,055 were in the untreated controls, 8,967 were in the GR24-treated group, and 7,569 were in the IBA-treated group. We subjected the DEGs of each group to k-means clustering analysis and classified them into 15 temporal expression patterns (Figure 2A–C). For the untreated controls, wound-responsive genes and plant hormone-related genes were specifically expressed in the early stage of AR formation (1M). Genes encoding auxin-responsive proteins and those relating to cell wall biogenesis and secondary metabolites were highly expressed 3 days (3M) and 7 days (7M) after rooting. Cell division and lateral organogenesis (*LBD*) genes were specifically upregulated at 7M (Figure 2A). For the IBA-treated cuttings, genes encoding auxin-responsive proteins and genes associated with cell division and *LBD* genes were upregulated earlier than those in the control group, which was consistent with the observed increase in AR formation after IBA treatment (Figure 2B). For the GR24-treated group, genes associated with wounding and hormone responses exhibited similar expression patterns to those in the control group. However, we observed three major differences in transcriptome changes in the GR24-treated group: (1) SLs signal transduction genes were upregulated, which is consistent with exogenous GR24 treatment; (2) genes

related to secondary metabolites, especially chlorophyll catabolic process, were expressed earlier in GR24-treated stems than those in the control group; (3) senescence-associated genes were upregulated in 3G and 7G (Figure 2C). These differences might explain the inhibitory effects of SLs on AR formation.

Next, we subjected transcriptomic data to pairwise comparisons within each time point (Figure S1). For all three treatments, the number of DEGs was higher at the later developmental stages of AR formation, suggesting that the effects of exogenous GR24 or IBA treatment were more pronounced at these stages. We investigated the DEGs that were inversely regulated between GR24- and IBA-treated groups for all three timepoints, to identify those genes specifically responsible for the inhibitory effects of SL (Figure 2E–G, Table S2). One day after rooting, 13 genes were downregulated in the 1G/1M comparison and were upregulated in the 1A/1M comparison (Figure 2E). Gene ontology (GO) enrichment analysis showed that "response to auxin" and "auxin-activated signaling pathway" were enriched, suggesting that SL inhibits auxin-mediated signaling during AR formation at early stages. Three days after rooting, 23 genes were downregulated in the 3G/3M comparison and were upregulated in the 3A/3M comparison (Figure 2F), and these genes had enriched GO terms mainly associated with "auxin-activated signaling pathway", "cellulose catabolic process". In contrast, four genes were upregulated in the 3G/3M comparison and were downregulated in the 3A/3M comparison, with enriched GO terms of "response to oxidative stress" and "peroxidase activity". Seven days after rooting, 192 genes were downregulated in the 7G/7M comparison and were upregulated in the 7A/7M comparison (Figure 2G), with enriched GO terms mainly associated with "auxin-activated signaling pathway", "cellulase activity", "pectate lyase activity", and "pectinesterase activity". Furthermore, 19 genes were upregulated in the 7G/7M comparison and downregulated in the 7A/7M comparison, with functions associated with "xyloglucan:xyloglucosyl transferase activity". These results suggest that SLs might suppress AR formation by inhibiting auxin-activated signaling pathways and promoting cell wall modification.

We further studied the functional differences among the treatments by subjecting the

DEGs from each comparison to MapMan enrichment analysis. “Transcription Factor” functions were also enriched among most of the comparisons (Figure S2). We further performed MapMan enrichment analysis specifically for the differentially expressed genes that encoded transcription factors (Figure 2H), and found those associated with root primordium formation were specifically upregulated in the IBA-treated group and downregulated in GR24-treated group. For instance, those encoding WUSCHEL-related homeobox (WOX) proteins, which promote cell division and organ development, and ASYMMETRIC LEAVES2/LATERAL ORGAN BOUNDARIES (AS2/LOB), which plays an important role in the regulation of organ development and metabolism, were enriched in the 3A/3M and 7A/7M comparisons. We also identified several transcription factors, which have been reported to regulate diverse aspects of plant growth and development. For example, NAC (NAM, ATAF1/2, CUC2), MYB and KNOX (Qin et al., 2020; Shanfa Lua et al., 2013). These results further demonstrate that SLs impact AR formation by regulate transcription factors expression level.

SLs altered the level of endogenous hormones during apple AR formation

The MapMan enrichment analysis identified several hormone-related transcription factors that were differentially expressed during AR formation. These include Type-B ARR (ARR-B) transcription factors involved in cytokinin signal transduction, ARFs, which regulate auxin-responsive genes by binding to auxin response elements (AuxREs), and APETALA2/ETHYLENE RESPONSE FACTORS (AP2/ERFs), which are associated with ethylene responses (Figure 2H, Figue S2). The k-means clustering analysis also identified genes relating to hormones, including auxin, cytokinin, ethylene, abscisic acid and jasmonic acid (Figure 2A–D). To study the roles of phytohormones in the inhibitory effects of SL on AR formation, we measured the levels of the hormones or their precursors: auxin (IAA), cytokinin (trans-Zeatin), gibberellins (GA_4), abscisic acid (ABA), ethylene (ACC), and jasmonic acid (JA) in untreated stem cuttings or those treated with GR24, at all four timepoints. We identified two types of changes among these analyzed hormones (Figure S3): (1) GR24-treatment influenced the levels of IAA, GA_4, and ABA at specific timepoints (Figure S3A–C). For instance, the concentration

of IAA was significantly reduced in GR24-treated stems 1 day after rooting, but the IAA content increased 3 days and 7 days after rooting. The change of the GA_4 content differed from that of the IAA content, and was reduced 1 day and 7 days after rooting, and increased 3 days after rooting. The ABA content only exhibited a significant reduction 3 days after rooting, and no changes were observed either 1 day or 7 days after rooting. (2) We observed increases in trans-zeatin, ACC, and SA following GR24 treatment at all three time points (Figure S3D–F).

Gene co-expression network analysis reveals the potential genes that mediated the inhibiting effect of SLs on AR formation

Transcriptome analysis showed that GR24-treatment altered the expression patterns of most of genes in apple during AR formation. It was obvious that one or more of these genes might play a dominant role in SLs inhibiting AR formation. To find out the genes, a weighted gene co-expression network analysis (WGCNA) was conducted by considering transcriptome data as well as the phenotypic data for AR formation (Figure 3A–D). After excluding non-expressed and lowly expressed genes, we identified 10 co-expression modules containing 6,176 DEGs (Figure 3A–B). The module–trait relationship showed that the 'blue' module was highly correlated with AR formation ($r = 0.97$, $P = 3 \times 10^{-18}$). Further analysis revealed that a total of 1,099 genes with an edge weight >0.20 were included in the 'blue' module. Among these genes, nine that were co-expressed and showed a high node connectivity (degree >42) were identified as hub genes, including *MdORE1*, *MdD14*, *MdCSLG3*, *MdACS*, *Mdperoxidase4*, *MdLAC3*, *MdLOG5, MdCCR1* and *MdEIN3* (Figure 3C). We further created a subnetwork that contained 102 genes whose encoded products had functions in cell wall biosynthesis, signal transduction, laccase and peroxidase, senescence-associated proteins, and transcriptional regulation, and identified two core hub genes, *ORESARA1* (MD06G1196100) and *LACCASE* (MD03G1056400) (Figure 3E–F).

Among the identified hub genes, *LACCASE* (*MdLAC3*) encodes a multicopper oxidoreductase that is associated with lignin deposition in xylem and *ORESARA1*

(*MdORE1*), encoding a NAC-domain transcription factor, is involved in plant senescence. These two hub genes might play important roles in the SL-mediated inhibition of root primordium formation and senescence during AR formation.

SLs promote cell wall growth during AR formation

Gene co-expression network and transcriptome analysis implied that SLs might suppress AR formation by adjusting cell wall growth. To characterize cell wall growth during AR formation, we cross-sectioned the base of the apple stem cuttings. Three days after rooting, we observed enhanced cell wall growth in control and GR24-treated stems, with a more pronounced growth in GR24-treated stems (Figure 4A). Seven days after rooting, stems of the control cuttings exhibited cell wall growth and root primordia, whereas GR24-treated stems showed more cell wall growth without initiating root primordia. By contrast, we observed no obvious cell wall growth for IBA-treated stems, but significantly more root primordia than untreated stems. The enhanced or reduced secondary cell wall in GR24- or IBA-treated stems, respectively, was also confirmed by transmission electron micrographs (Figure 4B-D). These results support the opposing role of SLs and auxin on root primordium and cell wall growth during AR formation. We also analyzed AR formation in an Arabidopsis SLs biosynthesis mutant, *max3*, which exhibited significantly more root primordia and enhanced AR formation than wild type, and GR24 treatment abolished AR formation in wild type and *max3* (Figure 4E–I). We also observed reduced lignin formation in *max3*, and GR24 treatment increased lignin formation in both wild type and *max3* (Figure 4J–M). These results suggested that SLs might inhibit AR formation via cell wall remodeling.

High-throughput sequencing of small RNAs and identification of miRNAs differentially expressed during AR formation

To identify miRNAs associated with the SL-mediated inhibition of AR formation, 30 small RNA libraries were constructed and sequenced. In total, 370.78 million reads were generated, ranging from 10.16 million to 16.68 million for each library. After cleaning and filtering of the sequences, approximately 79.12 million unique reads were

used for further analysis (Table 1). After removing the unqualified reads, we obtained reads among 18- to 25-nt sequences, and 24-nt (64.99%) small RNAs were the most abundant group, followed by 21-nt (17.74%), 22-nt (8.2%) and 23-nt small RNAs (3.11%) (Figure 5A; Figure S5). In total, 2,379 miRNAs were present in the data and these miRNAs were divided into six groups based their abundance in the miRNA database (Figure S6). Out of these miRNAs, 715 pre-miRNAs corresponding to 755 unique mature miRNAs were identified as known miRNAs, and all of these miRNAs belonged to 54 reported miRNA families (Figure S7). Among these miRNAs, those 21 nt in length accounted for 39.13%, and those 24 nt long for 22.27% (Table S3). In addition, 1,038 pre-miRNAs corresponding to 1,326 unique mature mRNAs were identified as novel miRNAs and those 24 nt in length accounted for 93.94% of these (Table S3). On the basis of Mfold Calculations, we observed that the Minimum Free Energy (MFE) of these novel miRNAs varied from −27.4 to −196.00 kcal mol^{-1}, and the MFE index ranged from 0.9 to 2.1 kcal mol^{-1}, confirming that the novel miRNAs could maintain stable hairpin structures.

We further subjected the identified known and novel miRNAs to pairwise comparisons within each time point (Figure 5C). In contrast to the transcriptome data, the miRNA data did not show significant more differentially expressed miRNAs at later development stages. However, similarly to the transcriptome analysis, we observed the highest number of differentially expressed miRNAs for 3A/3G or 7A/7G comparisons. Because auxin and SL have antagonistic effects on AR formation, we investigated the differentially expressed miRNAs that were inversely regulated between GR24- and IBA-treated groups for all three time points, to identify the miRNAs specifically responsible for the inhibitory effect of SL on AR formation (Figure 5D–F). We identified 31, 56, or 49 miRNAs that were inversely expressed between IBA- and GR24-treated groups 1, 3, or 7 days after rooting, respectively. These identified miRNAs represent ideal targets with which to analyze the function of miRNAs in the SL-mediated inhibition of AR formation.

miRNA target validation via degradome analysis and correlation analysis between

miRNAs and target genes

Degradome sequencing identified target genes by combining high-throughput sequencing and bioinformatic analysis, and can effectively avoid false-positive results (Q. Song, Liu, Hu, Zhang, & Ma, 2011). We constructed three pools using control samples (M), and those from the GR24 treatment (G) and IBA treatment (A), and 107.39 million raw reads were generated. After removing reads shorter than 15 nt, 106.78 million clean reads (99.44% of all reads) were mapped to 41,457 transcripts (91.89% of all 45,116 input transcripts). Integrated analysis verified 2,065 miRNA–mRNA pairs with 441 unique miRNAs (357 known and 84 novel) and 902 unique mRNA targets in the M pool, 2,074 miRNA–mRNA pairs with 468 unique miRNAs (378 known and 90 novel) and 964 unique mRNA targets in the G pool, and 2,691 miRNA–mRNA pairs with 500 unique miRNAs (395 known and 105 novel) and 1,278 unique mRNA targets in the A pool (Table S4). Overall, 586 miRNAs (448 known and 138 novel) were associated with 1,770 target genes. These targets were classified into five categories based on the abundance at each occupied transcript position (Yang & Chen, 2013); (Ambady, Wu, & Dominko, 2012; Han et al., 2016).

We further carried out GO enrichment analysis for the 1,770 targets (Figure 5G). And identify oxidoreductase activity (molecular function) and secondary metabolic process (biological process) as the top enriched terms. We used Cytoscape to create a network using miRNA–mRNA pairs with functions associated with root primordia and plant senescence. The network contained ARF genes and lignin biosynthesis-related genes (NAC, MYB). Notably, we identified *MdORE1*, which were also identified as core hub genes in the WGCNA (Figure 5H).

The differentially expressed miRNAs and DEGs between the GR24-treated and control groups at each timepoint were analyzed using the Pearson correlation coefficient. We identified a total of 373 (187 positive, 186 negative), 125 (66 positive, 59 negative), or 759 (371 positive, 388 negative) miRNA–mRNA interaction pairs at 1, 3, or 7 days after rooting, respectively (Figure 6A–B). A negative correlation indicates that a

miRNA and its target mRNA were differentially expressed after GR24 treatment. From these negatively correlated pairs, we identified 12 pairs with an inverse expression for mRNA and miRNA, including four, three, and six pairs for 1, 3, or 7 days after rooting, respectively (Figure S8). These pairs contained *MdORE1* and one laccase gene (*MdLAC3*). The expression of *MdORE1* was negatively correlated with mdm-miR164a or mdm-miR164b at 1 or 3 days after rooting, respectively, and expression of *MdLAC3* was negatively correlated with mdm-miR397 at 3 days after rooting. We have also employed the dual-luciferase sensor system to successfully verified the target relationship of these three miRNA–mRNA pairs: mdm-miR164a–*MdORE1* (Figure 7C and E), mdm-miR164b–*MdORE1* (Figure 7D and F) and mdm-miR397–*MdLAC3* (Figure S9B and C). These three miRNA–mRNA modules provide important guidance for the further characterization of the SL-mediated inhibition of AR formation. These three miRNA–mRNA modules provide important guidance for the further characterization of the SL-mediated inhibition of AR formation.

SLs regulate AR formation through mdm-miR164b-*MdORE1* module

Based on multi-omics analysis, we found mdm-miR164a/b was down-regulated by GR24 treatment during the critical period of AR formation. miR164 is a plant specific microRNA which had been extensively studied in regulating plant growth and development (J. Wang et al., 2021; Zhan et al., 2021). Therefore, miR164 might be largely involved in the SL mediated inhibition of AR formation. Since both mdm-miR164a and mdm-miR164b have the same target genes and the expression of mdm-miR164b had more severe reduction after GR24 treatment, we selected mdm-miR164b as the focus for further study. To investigate the role of mdm-miR164b during AR formation, transgenic tobacco plants overexpressing mdm-miR164b were produced. And significantly more ARs were observed in transgenic cuttings compared to wild type. Statistical analysis showed that overexpressing mdm-miR164b tobacco cuttings increased by an average of 30 ARs compared to the wild type (Figure 7K). These data verified that mdm-miR164b acts as a positive regulator of AR formation, and the

reduced expression of mdm-miR164b after GR24 treatment maybe a cause of the inhibited AR formation.

The module of mdm-miR164b–*MdORE1* has been verified both through multi-omics analysis and the dual-luciferase sensor system. In order to explore the role of *MdORE1* in SLs-mediated AR formation, we characterized the roles of *MdORE1* in details. Phylogenetic analysis indicated that *MdORE1*(MD06G1196100) was closely related to Arabidopsis *AtORE1* (Figure 8A). Subcellular localization analysis demonstrated that *MdORE1* localized in nucleus, which is consistent with its function of transcription factor (Figure 8B). In order to dissect the regulatory role of *MdORE1* on AR formation, we constructed a VIGS vector of *MdORE1*, and transformed into apple cuttings. The results showed that both rooting rates and roots number were significantly increased in TRV2-*MdORE1* transformation compared to control (Figure 8D-G). These results demonstrated that *MdORE1* played a negatively role in AR formation. Overall, our results suggest that SLs may inhibit AR formation through mdm-miR164-*MdORE1* module, that is to say, the reduced expression of mdm-miR164 caused by SLs treatment resulted in the upregulation of *MdORE1*, and leading to a decline of the rooting capacity of stem cuttings.

Discussion

In this study, we have used five *Malus* materials to demonstrate for the first time that SLs can inhibit AR formation in woody plants. Next, by employing the transgenic apple material, as well as WGCNA, we find SLs may inhibit AR formation by repressing the expression of cell fate transition genes and enhancing the expression of plant senescence genes. Furthermore, we were able to verify the role of mdm-miR164b-*MdORE1* module in the SLs-mediated inhibition of AR formation. Finally, these results led us delineate a molecular regulatory network and propose the potential cross-talk in SLs-mediated inhibition of AR formation. Our findings thus provide comprehensive insight into the function of SLs during AR formation, especially in woody plants.

Cell wall modification is involved in AR formation (Duman, Eliyahu, Abu-Abied, & Sadot, 2020). And in poplar, genes encoding cell wall-remodeling proteins, such as pectate lyases and pectin esterases, were highly expressed during the AR induction (Rigal et al., 2012). Auxin is a core player in the hormone cross-talk of AR formation and induces cellulase activity, which leads to the cleavage of cellulose chains and promotes cell wall loosening and extensibility (Abu-Abied et al., 2015). Furthermore, auxin triggers the demethylesterifcation of pectins and thereby lowers cell wall rigidity (Braybrook & Peaucelle, 2013). In this study, genes encoding cellulases (which catalyze the breakdown of cellulose), pectate lyases (which degrade pectins by cleaving α-1,4-galacturonosidic linkages), or pectinesterase (which catalyzes the hydrolysis of pectins), were upregulated by IBA treatment. These results support the importance of cell wall modification in AR formation. By contrast, the same genes were downregulated by GR24 treatment, suggesting that SLs regulate AR formation via cell wall modification (Figure 2E–F). We also observed enhanced lignin deposition after GR24 treatment. Lignin is a phenolic compound, and lignified cell walls usually inhibit the expansion and differentiation of plant cells (Mnich et al., 2020). In plants, lignin biosynthesis involves two key steps and multiple enzymes. Initially, three types of monolignols (G-, S- and H-type lignin) are synthesized from phenylalanine (Xue et al., 2019), and then peroxidase or LAC enzymes catalyze the polymerization of these three monolignols into lignin (L. Li et al., 2020; Shanfa Lua et al., 2013). The transcriptome analysis here showed that *LAC3* was more highly expressed following GR24 treatment. The miRNA and degradome analysis also identified mdm-miR397, which targets *MdLAC3,* as downregulated by GR24 treatment. Therefore, further characterization of mdm-miR397–*MdLAC3* module might potentially reveal the molecular mechanism of SLs-mediated enhancement of lignin biosynthesis during AR formation.

Age is a major determinant of regeneration and AR formation gradually decreased with increasing plant age (M. Xu et al., 2016). Plant aging is a complex biological process and is mediated by factors such as photoperiod, stress and phytohormones. It has been reported that SLs regulate plant aging (Yamada et al., 2014; Z. Zhang & Guo, 2018).

The blocking of SLs signaling transduction pathways in the rice *d3* mutant caused delayed leaf senescence (Yan et al., 2007) and in petunia and *Lotus japonicus*, SLs-insensitive mutants also showed delayed senescence (J. Liu et al., 2013; Snowden et al., 2005). SLs participate in leaf senescence via cross-talk with ethylene, and exogenous treatments with both ethylene and SLs stimulate leaf senescence more than treatment with either hormone alone (Mostofa, Li, Nguyen, Fujita, & Tran, 2018). In this study, we found the apple cuttings under GR24 treatment exhibited a certain amount of aging phenotype, including yellow leaf, decreased water content, reduced biomass (Figure S4), which is consistent with the reported functions. miR164 had been verified as the post-transcriptional regulator to guide the cleavage of the mRNAs of some NAC transcription factors and affect a range of plant traits including lateral root formation and plant senescence (Z. Li, Peng, Wen, & Guo, 2013; L. Zhang et al., 2018). In this study, we found GR24 treatment could inhibit the expression of mdm-miR164a/b during AR formation (Figure 7G-K). Over expression of apple mdm-miR164 in tobacco showed enhanced AR formation compared to control. Therefore, we preliminarily speculated that SLs may reduce the AR forming capacity by regulating the mdm-miR164 expression level.

ORESARA1(*ORE1*) is a kind of NAC transcription factor, and overexpression of *ORE1* was reported to accelerate aging, while ore1 mutant showed delayed senescence (Kim et al., 2018). In addition, *ORE1* is a target gene of miR164, which interacts with *ORE1* mRNA to promote its degradation. Our multi-omics analysis showed that GR24 treatment led to a significantly increased expression of *MdORE1* (Figure 6C–D). Through employing the virus-induced gene silencing (VIGS) technology, we were able to silence the *MdORE1* orthologue in apple and observed significantly increased AR number in the VIGS lines compared to control (Figure 8F-G). And we have also demonstrated the target relationship of mdm-miR164a–*MdORE1* and mdm-miR164b–*MdORE1* by using degradome sequencing and a dual-luciferase sensor system（Figure 7）. Overall, our results support that the mdm-miR164a/b-*MdORE1* module provides

a novel regulatory pathway for SLs signaling to inhibit AR formation.

The GR24 treatment also significantly increased endogenous ethylene content and enhanced the expression of the ethylene biosynthesis gene, *MdACS4-like* and ethylene signal transduction gene, *ETHYLENE INSENSITIVE 3* (*EIN3*) (Figure S3E and S10). Plants with high *EIN3* expression had reduced expression levels of *WOX11* and *WOX5*, resulting in reduced regeneration ability (H. Li, Yao, Sun, & Zhu, 2020). Furthermore, *EIN3* has been shown to accelerate age-dependent senescence by directly repressing miR164 transcription (Z. Li et al., 2013). Therefore, ethylene may also play important roles in the SLs-mediated AR formation.

AR formation is crucial for the successful vegetative propagation of woody plants, including horticultural and forestry crops (Stevens, Woeste, & Pijut, 2018). The enhancement of AR formation via genetic engineering approaches has been accomplished for several species (Q. J. Chen et al., 2020; Sukumar, Maloney, & Muday, 2013). However, most of these strategies are about overexpression of genes such as *rolB* and *iaaM* (W. Li et al., 2017; Welander, Pawlicki, Holefors, & Wilson, 1998) and might cause public concerns over transgene flow and food safety (W. Li et al., 2019). The creation of targeted mutations by CRISPR technology has been widely used for crop improvement. More importantly, CRISPR components and target mutations can be segregated through either sexually propagation or using transient transformation system, to produce mutants with no CRISPR components (L. Chen et al., 2018). Here, we have demonstrated that SLs inhibit AR formation, and have identified several genes that negatively regulate AR formation. These genes are ideal targets for increasing AR formation via CRISPR technology. For example, sgRNAs can be designed to target the orthologs of SL biosynthesis genes in apple, *MdCCD7* or *MdCCD8*, to reduce the endogenous SL level (Foster et al., 2018). These SL biosynthesis mutants might display enhanced AR formation because of the absence of SL inhibition. These potential mutants might also be non-transgenic if the *Agrobacterium*-mediated transient CRISPR expression system is used.

Acknowledgements

This work was supported by the National Natural Science Foundation of China (31801823), the National Key Research and Development Program (2018YFD1000100), the earmarked fund for the China Agricultural Research System (CARS-27), 2115 Talent Development Program of China Agricultural University, and the Construction of Beijing Science and Technology Innovation and Service Capacity in Top Subjects (CEFF-PXM2019_014207_000032).

References

Abarca, D., Pizarro, A., Amo, A., & Diaz-Sala, C. (2011). Screening of genes associated with early stages of adventitious root formation from progenitor adult cells of pine. *BMC Proceedings, 5*(Suppl 7), P133. doi:10.1186/1753-6561-5-s7-p133

Abu-Abied, M., Rogovoy Stelmakh, O., Mordehaev, I., Grumberg, M., Elbaum, R., Wasteneys, G. O., & Sadot, E. (2015). Dissecting the contribution of microtubule behaviour in adventitious root induction. *J Exp Bot, 66*(9), 2813-2824. doi:10.1093/jxb/erv097

Addo-Quaye, C., Miller, W., & Axtell, M. J. (2009). CleaveLand: a pipeline for using degradome data to find cleaved small RNA targets. *Bioinformatics, 25*(1), 130-131. doi:10.1093/bioinformatics/btn604

Alexa, A., & Rahnenfuhrer, J. (2010). topGO: Enrichment analysis for Gene Ontology. *R package version*, 2.8.

Amano, R., Nakayama, H., Momoi, R., Omata, E., Gunji, S., Takebayashi, Y., . . . Kimura, S. (2020). Molecular Basis for Natural Vegetative Propagation via Regeneration in North American Lake Cress, Rorippa aquatica (Brassicaceae). *Plant Cell Physiol, 61*(2), 353-369. doi:10.1093/pcp/pcz202

Ambady, S., Wu, Z., & Dominko, T. (2012). Identification of novel microRNAs in Xenopus laevis metaphase II arrested eggs. *Genesis, 50*(3), 286-299. doi:10.1002/dvg.22010

An, J. P., Zhang, X. W., Bi, S. Q., You, C. X., Wang, X. F., & Hao, Y. J. (2019). MdbHLH93, an apple activator regulating leaf senescence, is regulated by ABA and MdBT2 in antagonistic ways. *New Phytol, 222*(2), 735-751. doi:10.1111/nph.15628

Anders, S., & Huber, W. (2010). Differential expression analysis for sequence count data. . *11*, R106.

Atkinson, J. A., Rasmussen, A., Traini, R., Voss, U., Sturrock, C., Mooney, S. J., . . . Bennett, M. J. (2014). Branching Out in Roots: Uncovering Form, Function, and Regulation. *Plant Physiol, 166*(2), 538-550. doi:10.1104/pp.114.245423

Bellini, C., Pacurar, D. I., & Perrone, I. (2014). Adventitious roots and lateral roots: similarities and differences. *Annu Rev Plant Biol, 65*, 639-666. doi:10.1146/annurev-arplant-050213-035645

Birnbaum, K. D., & Sanchez Alvarado, A. (2008). Slicing across kingdoms: regeneration in plants and animals. *Cell, 132*(4), 697-710. doi:10.1016/j.cell.2008.01.040

Braybrook, S. A., & Peaucelle, A. (2013). Mechano-chemical aspects of organ formation in *Arabidopsis thaliana*: the relationship between auxin and pectin. *PLoS One, 8*(3), e57813. doi:10.1371/journal.pone.0057813

Brewer, P. B., Koltai, H., & Beveridge, C. A. (2013). Diverse roles of strigolactones in plant development. *Mol Plant, 6*(1), 18-28. doi:10.1093/mp/sss130

Cai, H., Yang, C., Liu, S., Qi, H., Wu, L., Xu, L. A., & Xu, M. (2019). MiRNA-target pairs regulate adventitious rooting in Populus: a functional role for miR167a and its target Auxin response factor 8. *Tree Physiol, 39*(11), 1922-1936. doi:10.1093/treephys/tpz085

Chen, C., Chen, H., Zhang, Y., Thomas, H. R., Frank, M. H., He, Y., & Xia, R. (2020). TBtools - an integrative toolkit developed for interactive analyses of big biological data. *Mol Plant*. doi:10.1016/j.molp.2020.06.009

Chen, J., Li, Y., Li, Y., Li, Y., Wang, Y., Jiang, C., . . . Ma, N. (2021). AUXIN RESPONSE FACTOR 18-HISTONE DEACETYLASE 6 module regulates floral organ identity in rose (Rosa hybrida). *Plant Physiol*. doi:10.1093/plphys/kiab130

Chen, L., Li, W., Katin-Grazzini, L., Ding, J., Gu, X., Li, Y., . . . Li, Y. (2018). A method for the production and expedient screening of CRISPR/Cas9-mediated non-transgenic mutant plants. *Hortic Res, 5*, 13. doi:10.1038/s41438-018-0023-4

Chen, Q. J., Deng, B. H., Gao, J., Zhao, Z. Y., Chen, Z. L., Song, S. R., . . . Wang, S. P. (2020). A miRNA-Encoded Small Peptide, vvi-miPEP171d1, Regulates Adventitious Root Formation. *Plant Physiol, 183*(2), 656-670. doi:10.1104/pp.20.00197

Chen, W., Gai, Y., Liu, S., Wang, R., & Jiang, X. (2010). Quantitative analysis of cytokinins in plants by high performance liquid chromatography: electronspray ionization ion trap mass spectrometry. *J Integr Plant Biol, 52*(10), 925-932. doi:10.1111/j.1744-7909.2010.00989.x

da Costa, C. T., de Almeida, M. R., Ruedell, C. M., Schwambach, J., Maraschin, F. S., & Fett-Neto, A. G. (2013). When stress and development go hand in hand: main hormonal controls of adventitious rooting in cuttings. *Front Plant Sci, 4*, 133. doi:10.3389/fpls.2013.00133

Damodharan, S., Corem, S., Gupta, S. K., & Arazi, T. (2018). Tuning of SlARF10A dosage by sly-miR160a is critical for auxin-mediated compound leaf and flower development. *Plant J, 96*(4), 855-868. doi:10.1111/tpj.14073

Della Rovere, F., Fattorini, L., D'Angeli, S., Veloccia, A., Falasca, G., & Altamura, M. M. (2013). Auxin and cytokinin control formation of the quiescent centre in the adventitious root apex of Arabidopsis. *Ann Bot, 112*(7), 1395-1407. doi:10.1093/aob/mct215

Duan, J., Yu, H., Yuan, K., Liao, Z., Meng, X., Jing, Y., . . . Li, J. (2019). Strigolactone promotes cytokinin degradation through transcriptional activation of CYTOKININ OXIDASE/DEHYDROGENASE 9 in rice. *Proc Natl Acad Sci U*

S A, 116(28), 14319-14324. doi:10.1073/pnas.1810980116

Duman, Z., Eliyahu, A., Abu-Abied, M., & Sadot, E. (2020). The contribution of cell wall remodeling and signaling to lateral organs formation. *Israel Journal of Plant Sciences, 67*(1-2), 110-127. doi:10.1163/22238980-20191115

Foster, T. M., Ledger, S. E., Janssen, B. J., Luo, Z., Drummond, R. S. M., Tomes, S., . . . Snowden, K. C. (2018). Expression of MdCCD7 in the scion determines the extent of sylleptic branching and the primary shoot growth rate of apple trees. *J Exp Bot, 69*(9), 2379-2390. doi:10.1093/jxb/erx404

Gamir, J., Torres-Vera, R., Rial, C., Berrio, E., de Souza Campos, P. M., Varela, R. M., . . . Lopez-Raez, J. A. (2020). Exogenous strigolactones impact metabolic profiles and phosphate starvation signalling in roots. *Plant Cell Environ, 43*(7), 1655-1668. doi:10.1111/pce.13760

Gomez-Roldan, V., Fermas, S., Brewer, P. B., Puech-Pages, V., Dun, E. A., Pillot, J. P., . . . Rochange, S. F. (2008). Strigolactone inhibition of shoot branching. *Nature, 455*(7210), 189-194. doi:10.1038/nature07271

Gutierrez, L., Bussell, J. D., Pacurar, D. I., Schwambach, J., Pacurar, M., & Bellini, C. (2009). Phenotypic plasticity of adventitious rooting in Arabidopsis is controlled by complex regulation of AUXIN RESPONSE FACTOR transcripts and microRNA abundance. *Plant Cell, 21*(10), 3119-3132. doi:10.1105/tpc.108.064758

Gutierrez, L., Mongelard, G., Flokova, K., Pacurar, D. I., Novak, O., Staswick, P., . . . Bellini, C. (2012). Auxin controls Arabidopsis adventitious root initiation by regulating jasmonic acid homeostasis. *Plant Cell, 24*(6), 2515-2527. doi:10.1105/tpc.112.099119

Han, X., Yin, H., Song, X., Zhang, Y., Liu, M., Sang, J., . . . Zhuo, R. (2016). Integration of small RNAs, degradome and transcriptome sequencing in hyperaccumulatorSedum alfrediiuncovers a complex regulatory network and provides insights into cadmium phytoremediation. *Plant Biotechnology Journal, 14*(6), 1470-1483. doi:10.1111/pbi.12512

Kang, W., Li, R., Liyuan, W., & Hao, C. (2019). Auxin-Induced Adventitious Root Formation in Nodal Cuttings of Camellia sinensis. *Int J Mol Sci, 20*(19), 4817. doi:10.3390/ijms20194817

Kim, H., Kim, H. J., Vu, Q. T., Jung, S., McClung, C. R., Hong, S., & Nam, H. G. (2018). Circadian control of ORE1 by PRR9 positively regulates leaf senescence in Arabidopsis. *Proc. Natl. Acad. Sci. U.S.A., 115*, 8448-8453.

Klerk, G.-J. D., B, A.-S., R, L., & KH, N. (1997). Regeneration of roots, shoots and embryos: physiological, biochemical and molecular aspects. *Biol Plant, 39*, 53-66.

Kohlen, W., Charnikhova, T., Lammers, M., Pollina, T., Toth, P., Haider, I., . . . Lopez-Raez, J. A. (2012). The tomato CAROTENOID CLEAVAGE DIOXYGENASE8 (SlCCD8) regulates rhizosphere signaling, plant architecture and affects reproductive development through strigolactone biosynthesis. *New Phytol, 196*(2), 535-547. doi:10.1111/j.1469-8137.2012.04265.x

Legué, V., Rigald, A., & Bhaleraod, R. P. (2014). Adventitious root formation in tree species: involvement of transcription factors. *Physiol Plant, 151*(2), 192-198. doi:10.1111/ppl.12197

Li, H., Yao, L., Sun, L., & Zhu, Z. (2020). ETHYLENE INSENSITIVE 3 suppresses plant de novo root regeneration from leaf explants and mediates age-regulated regeneration decline. *Development, 147*(9). doi:10.1242/dev.179457

Li, K., Liu, Z., Xing, L., Wei, Y., Mao, J., Meng, Y., . . . Zhang, D. (2019). miRNAs associated with auxin signaling, stress response, and cellular activities mediate adventitious root formation in apple rootstocks. *Plant Physiol Biochem, 139*, 66-81. doi:10.1016/j.plaphy.2019.03.006

Li, L., Yang, K., Wang, S., Lou, Y., Zhu, C., & Gao, Z. (2020). Genome-wide analysis of laccase genes in moso bamboo highlights PeLAC10 involved in lignin biosynthesis and in response to abiotic stresses. *Plant Cell Rep, 39*(6), 751-763. doi:10.1007/s00299-020-02528-w

Li, W., Fang, C., Krishnan, S., Chen, J., Yu, H., Murphy, A. S., . . . Li, Y. (2017). Elevated auxin and reduced cytokinin contents in rootstocks improve their performance and grafting success. *Plant Biotechnol J, 15*(12), 1556-1565. doi:10.1111/pbi.12738

Li, W., Zhai, L., Strauss, S. H., Yer, H., Merewitz, E., Chen, J., . . . Li, Y. (2019). Transgenic Reduction of Cytokinin Levels in Roots Inhibits Root-Sprouting in Populus. *Plant Physiol, 180*(4), 1788-1792. doi:10.1104/pp.19.00217

Li, Z., Peng, J., Wen, X., & Guo, H. (2013). Ethylene-insensitive3 is a senescence-associated gene that accelerates age-dependent leaf senescence by directly repressing miR164 transcription in Arabidopsis. *Plant Cell, 25*(9), 3311-3328. doi:10.1105/tpc.113.113340

Liu, J., Novero, M., Charnikhova, T., Ferrandino, A., Schubert, A., Ruyter-Spira, C., . . . Cardinale, F. (2013). Carotenoid cleavage dioxygenase 7 modulates plant growth, reproduction, senescence, and determinate nodulation in the model legume Lotus japonicus. *J Exp Bot, 64*(7), 1967-1981. doi:10.1093/jxb/ert056

Liu, Q., Wang, F., & Axtell, M. J. (2014). Analysis of complementarity requirements for plant microRNA targeting using a Nicotiana benthamiana quantitative transient assay. *Plant Cell, 26*(2), 741-753. doi:10.1105/tpc.113.120972

Liu, S., Chen, W., Qu, L., Gai, Y., & Jiang, X. (2013). Simultaneous determination of 24 or more acidic and alkaline phytohormones in femtomole quantities of plant tissues by high-performance liquid chromatography-electrospray ionization-ion trap mass spectrometry. *Analatical Bioanalytical Chemistry, 405*, 1257-1266. doi:10.1007/s00216-012-6509-2)

Liu, S., Yang, C., Wu, L., Cai, H., Li, H., & Xu, M. (2020). The peu-miR160a-PeARF17.1/PeARF17.2 module participates in the adventitious root development of poplar. *Plant Biotechnol J, 18*(2), 457-469. doi:10.1111/pbi.13211

Lopez-Raez, J. A., Shirasu, K., & Foo, E. (2017). Strigolactones in Plant Interactions with Beneficial and Detrimental Organisms: The Yin and Yang. *Trends Plant Sci, 22*(6), 527-537. doi:10.1016/j.tplants.2017.03.011

Ludwig-Muller, J., Vertocnik, A., & Town, C. D. (2005). Analysis of indole-3-butyric acid-induced adventitious root formation on Arabidopsis stem segments. *J Exp Bot, 56*(418), 2095-2105. doi:10.1093/jxb/eri208

Majer, C., Xu, C., Berendzen, K. W., & Hochholdinger, F. (2012). Molecular interactions of ROOTLESS CONCERNING CROWN AND SEMINAL ROOTS, a LOB domain protein regulating shoot-borne root initiation in maize (Zea mays L.). *Philos Trans R Soc Lond B Biol Sci, 367*(1595), 1542-1551. doi:10.1098/rstb.2011.0238

Mehrotra, R., Bhalothia, P., Bansal, P., Basantani, M. K., Bharti, V., & Mehrotra, S. (2014). Abscisic acid and abiotic stress tolerance - different tiers of regulation. *J Plant Physiol, 171*(7), 486-496. doi:10.1016/j.jplph.2013.12.007

Mnich, E., Bjarnholt, N., Eudes, A., Harholt, J., Holland, C., Jorgensen, B., . . . Ulvskov, P. (2020). Phenolic cross-links: building and de-constructing the plant cell wall. *Nat Prod Rep*. doi:10.1039/c9np00028c

Mostofa, M. G., Li, W., Nguyen, K. H., Fujita, M., & Tran, L. P. (2018). Strigolactones in plant adaptation to abiotic stresses: An emerging avenue of plant research. *Plant Cell Environ, 41*(10), 2227-2243. doi:10.1111/pce.13364

Muday, G. K., Rahman, A., & Binder, B. M. (2012). Auxin and ethylene: collaborators or competitors? *Trends Plant Sci, 17*(4), 181-195. doi:10.1016/j.tplants.2012.02.001

Negi, S., Sukumar, P., Liu, X., Cohen, J. D., & Muday, G. K. (2010). Genetic dissection of the role of ethylene in regulating auxin-dependent lateral and adventitious root formation in tomato. *Plant J, 61*(1), 3-15. doi:10.1111/j.1365-313X.2009.04027.x

Okushima, Y., Fukaki, H., Onoda, M., Theologis, A., & Tasaka, M. (2007). ARF7 and ARF19 regulate lateral root formation via direct activation of LBD/ASL genes in Arabidopsis. *Plant Cell, 19*(1), 118-130. doi:10.1105/tpc.106.047761

Qin, W., Yin, Q., Chen, J., Zhao, X., Yue, F., He, J., . . . Wu, A. M. (2020). The Class II KNOX transcription factors KNAT3 and KNAT7 synergistically regulate monolignol biosynthesis in Arabidopsis. *J Exp Bot, eraa266*. doi:10.1093/jxb/eraa266

Rasmussen, A., Mason, M. G., De Cuyper, C., Brewer, P. B., Herold, S., Agusti, J., . . . Beveridge, C. A. (2012). Strigolactones Suppress Adventitious Rooting in Arabidopsis and Pea. *Plant Physiol, 158*(4), 1976-1987. doi:10.1104/pp.111.187104

Rigal, A., Yordanov, Y. S., Perrone, I., Karlberg, A., Tisserant, E., Bellini, C., . . . Legue, V. (2012). The AINTEGUMENTA LIKE1 homeotic transcription factor PtAIL1 controls the formation of adventitious root primordia in poplar. *Plant Physiol, 160*(4), 1996-2006. doi:10.1104/pp.112.204453

Shanfa Lua, Q. L., Hairong Weid, Mao-Ju Change, Sermsawat Tunlaya-Anukitb, Hoon Kimf, Jie Liub,, Jingyuan Songa, Y.-H. S., Lichai Yuana, Ting-Feng Yehe, Ilona Peszlenh, John Ralphf, Ronald R. Sederoffb,, & Chiangb, V. L. (2013). Ptr-miR397a is a negative regulator of laccase genes affecting lignin content in Populus trichocarpa. *110*, 10848–10853.

Snowden, K. C., Simkin, A. J., Janssen, B. J., Templeton, K. R., Loucas, H. M., Simons, J. L., . . . Klee, H. J. (2005). The Decreased apical dominance1/Petunia hybrida CAROTENOID CLEAVAGE DIOXYGENASE8 gene affects branch production and plays a role in leaf senescence, root growth, and flower development. *Plant Cell, 17*(3), 746-759. doi:10.1105/tpc.104.027714

Song, D., Shen, J., & Li, L. (2010). Characterization of cellulose synthase complexes in Populus xylem differentiation. *New Phytol, 187*(3), 777-790. doi:10.1111/j.1469-8137.2010.03315.x

Song, Q., Liu, Y., Hu, X., Zhang, W., & Ma, B. (2011). Identification of miRNAs and their target genes in developing soybean seeds by deep sequencing. *BMC Plant Biology, 11*, 5.

SPEE, E. (1987). A method of retaining phloroglucinol proof of lignin. *Stain Technol, 62(4)*, 279-280.

Stevens, M. E., Woeste, K. E., & Pijut, P. M. (2018). Localized gene expression changes during adventitious root formation in black walnut (Juglans nigra L.). *Tree Physiol, 38*(6), 877-894. doi:10.1093/treephys/tpx175

Sukumar, P., Maloney, G. S., & Muday, G. K. (2013). Localized induction of the ATP-binding cassette B19 auxin transporter enhances adventitious root formation in Arabidopsis. *Plant Physiol, 162*(3), 1392-1405. doi:10.1104/pp.113.217174

Umehara, M., Hanada, A., Yoshida, S., Akiyama, K., Arite, T., Takeda-Kamiya, N., . . . Yamaguchi, S. (2008). Inhibition of shoot branching by new terpenoid plant hormones. *Nature, 455*(7210), 195-200. doi:10.1038/nature07272

Wang, J., Bao, J., Zhou, B., Li, M., Li, X., & Jin, J. (2021). The osa-miR164 target OsCUC1 functions redundantly with OsCUC3 in controlling rice meristem/organ boundary specification. *New Phytol, 229*(3), 1566-1581. doi:10.1111/nph.16939

Wang, Z., Gerstein, M., & Snyder, M. (2009). RNA-Seq: a revolutionary tool for transcriptomics. *10*, 57-63.

Wang, Z., Hua, J., Yin, Y., Gu, C., Yu, C., Shi, Q., . . . Yu, F. (2019). An Integrated Transcriptome and Proteome Analysis Reveals Putative Regulators of Adventitious Root Formation in Taxodium 'Zhongshanshan'. *Int J Mol Sci, 20*(5), 1225. doi:10.3390/ijms20051225

Welander, M., Pawlicki, N., Holefors, A., & Wilson, F. (1998). Genetic transformation of the apple rootstock M26 with the RolB gene and its influence on rooting. *Journal of Plant Physiology, 153*(3-4), 371-380. doi:10.1016/s0176-1617(98)80164-8

Xu, M., Hu, T., Zhao, J., Park, M. Y., Earley, K. W., Wu, G., . . . Poethig, R. S. (2016). Developmental Functions of miR156-Regulated SQUAMOSA PROMOTER BINDING PROTEIN-LIKE (SPL) Genes in *Arabidopsis thaliana*. *PLoS Genet, 12*(8), e1006263. doi:10.1371/journal.pgen.1006263

Xu, X., Li, X., Hu, X., Wu, T., Wang, Y., Xu, X., . . . Han, Z. (2017). High miR156 Expression Is Required for Auxin-Induced Adventitious Root Formation via MxSPL26 Independent of PINs and ARFs in Malus xiaojinensis. *Front Plant Sci, 8*, 1059. doi:10.3389/fpls.2017.01059

Xue, C., Yao, J.-L., Qin, M.-F., Zhang, M.-Y., Allan, A. C., Wang, D.-F., & Wu, J. (2019). PbrmiR397a regulates lignification during stone cell development in pear fruit. *Plant Biotechnology Journal, 17*(1), 103-117. doi:10.1111/pbi.12950

Yamada, Y., Furusawa, S., Nagasaka, S., Shimomura, K., Yamaguchi, S., & Umehara, M. (2014). Strigolactone signaling regulates rice leaf senescence in response to a phosphate deficienc. *Planta, 240*, 399-408. doi:10.1007/s00425-014-2096-0)

Yan, H., Saika, H., Maekawa, M., Takamure, I., Tsutsumi, N., Kyozuka1, J., & Nakazono, M. (2007). Rice tillering dwarf mutant dwarf3 has increased leaf longevity during darkness-induced senescence or hydrogen peroxide-induced cell death. *Genes Genet. Syst, 82*, 361–366.

Yang, Z. M., & Chen, J. (2013). A potential role of microRNAs in plant response to metal toxicity. *Metallomics, 5*(9), 1184-1190. doi:10.1039/c3mt00022b

You, C. X., Zhao, Q., Wang, X. F., Xie, X. B., Feng, X. M., Zhao, L. L., . . . Hao, Y. J. (2014). A dsRNA-binding protein MdDRB1 associated with miRNA biogenesis modifies adventitious rooting and tree architecture in apple. *Plant Biotechnol J, 12*(2), 183-192. doi:10.1111/pbi.12125

Zhan, J., Chu, Y., Wang, Y., Diao, Y., Zhao, Y., Liu, L., . . . Ge, X. (2021). The miR164-GhCUC2-GhBRC1 module regulates plant architecture through abscisic acid in cotton. *Plant Biotechnol J*. doi:10.1111/pbi.13599

Zhang, L., Yao, L., Zhang, N., Yang, J., Zhu, X., Tang, X., . . . Si, H. (2018). Lateral Root Development in Potato Is Mediated by Stu-mi164 Regulation of NAC Transcription Factor. *Front Plant Sci, 9*, 383. doi:10.3389/fpls.2018.00383

Zhang, M., An, P., Li, H., Wang, X., Zhou, J., Dong, P., . . . Li, C. (2019). The miRNA-Mediated Post-Transcriptional Regulation of Maize in Response to High Temperature. *Int J Mol Sci, 20*(7). doi:10.3390/ijms20071754

Zhang, Z., & Guo, Y. (2018). Hormone Treatments in Studying Leaf Senescence. *Methods Mol Biol, 1744*, 125-132. doi:10.1007/978-1-4939-7672-0_11

Zhao, Y., Christensen, S. K., Fankhause, C., Cashman, J. R., Cohen, J. D., Weigel, D., & Chory, J. (2001). A role for flavin monooxygenase-like enzymes in auxin biosynthesis. *Science, 291*, 306-309.

Zhao, J., Jiang, L., Che, G., Pan, Y., Li, Y., Hou, Y., . . . Zhang, X. (2019). A Functional Allele of CsFUL1 Regulates Fruit Length through Repressing CsSUP and Inhibiting Auxin Transport in Cucumber. *Plant Cell, 31*(6), 1289-1307. doi:10.1105/tpc.18.00905

Zheng, L., Nagpal, P., Villarino, G., Trinidad, B., Bird, L., Huang, Y., & Reed, J. W. (2019). miR167 limits anther growth to potentiate anther dehiscence. *Development, 146*(14), dev174375. doi:10.1242/dev.174375

Zheng, X., Deng, W., Luo, K., Duan, H., Chen, Y., McAvoy, R., . . . Li, Y. (2007). The cauliflower mosaic virus (CaMV) 35S promoter sequence alters the level and patterns of activity of adjacent tissue- and organ-specific gene promoters. *Plant Cell Rep, 26*(8), 1195-1203. doi:10.1007/s00299-007-0307-x

Legends

Table 1. The small RNA sequencing data generated for 30 samples using Illumina sequencing platform.

Figure 1. Adventitious root (AR) formation of *Malus* stem cuttings. (A) Complete inhibition of AR formation was observed at GR24 concentrations higher than 10 μM for M26 and Royal Gala. (B–D) Rooting efficiency (B), AR number (C), and AR length (D) of all five *Malus* materials either without treatment, or with 10 μM GR24 treatment, 0.3 mg L^{-1} IBA treatment or 10 μM GR24 + 0.3 mg L^{-1} IBA treatment. (E–H) Phenotype of M26 stem cuttings in control medium (E) or medium with 10 μM GR24 (F), 0.3 mg L^{-1} IBA (G) or 10 μM GR24 + 0.3 mg/L^{-1} IBA (H) for two weeks. (I–J). Phenotype of Royal Gala stem cuttings in control medium (I), or medium with 10 μM GR24 (J), 0.3 mg L^{-1} IBA (K) or 10 μM GR24 + 0.3 mg L^{-1} IBA (L) for two weeks. Bars represent 0.5 cm. The data for each time point are means for three biological replicates ± SE.

Figure 2. Gene expression profiles and functional clustering over the time-course of AR formation under different treatments. (A–C) Heatmaps showing the gene expression profiles in k-means clusters without treatment (A), with IBA treatment (B) or with GR24 treatment (C). Red indicates higher expression, and green indicates low expression. (D) A schematic diagram of gene functional changes during AR formation under different treatments. The red lines show genes with reduced expression levels during AR formation and blue lines show genes with enhanced expression levels. (E–G) Identification of DEGs inversely regulated between GR24- and IBA-treated groups at 1 day (E), 3 days (F), or 7 days (G) after rooting. The overlapping region of the Venn diagrams represents DEGs that have the opposite expression pattern in IBA and GR24 treatments. The heatmap shows the expression level of each DEG in the overlapping region. (H) MapMan enrichment for transcription factor (TF) genes identified from the DEGs. The heatmap shows the level of enrichment for each category of TF. M: control; G: 10μM GR24-treatment; A: 0.3 mg L^{-1} IBA treatment.

Figure 3. Figure 3. Co-expression network analysis of DEGs involved in AR formation. (A) Clustering dendrogram based on the dissimilarity topological overlap of genes across all samples. (B) Relationship between each module and each selected trait. The correlation value for each module–trait pair is shown from −1 (green) to 1 (red). The *P*-value for each module-trait comparison is displayed in parentheses. (C) In the blue module, nine co-expressed genes with a high node connectivity were identified (yellow circle). (D) Two hub genes (*MdLaccase* and *MdORE1*) were identified from a sub-network with 102 functional genes in the blue module.

Figure 4. Anatomical observations of AR formation in apple stem cuttings. (A) Paraffin-embedded sections of apple stem cuttings without treatment, or with 10 μM GR24 treatment or 0.3 mg L^{-1} IBA treatment at all four timepoints. Black arrows represent root primordia and red arrows and lines represent enhanced cell wall growth. (B-D) Transmission electron micrographs of apple stem cuttings in the rooting medium without treatment (B), or with 10 μM GR24 (C) or 0.3 mg L^{-1} IBA treatment (D), bars

= 0.5 μm. (E) Rooting ability of Arabidopsis WT and *max3* after 10 days in rooting medium. (F–I) Scanning electron micrographs of WT and *max3* mutant without treatment (F: WT; G: *max3*) or with 5 μM GR24 treatment (H: WT; I: *max3*) for 5 days. Yellow highlights represent ARs. Bars = 0.7 mm. (J–M) Histochemical staining with phloroglucinol-HCl for Arabidopsis WT and *max3* without treatment (J: WT; K: *max3*) or with 5 μM GR24 treatment (L: WT; M: *max3*) for 5 days. Bars = 0.1 mm.

Figure 5. Sequencing analysis of small RNAs and the degradome. (A) A pie chart showing the length distribution of the identified small RNAs. (B) The circles show the distribution of known and novel small RNAs in the apple genome. The outermost circle represents the different chromosomes in the apple genome. From outer to inner, the circles represent known miRNAs (green) and novel miRNAs (blue). (C) Bar plot showing the number of DEGs for pairwise comparisons within each timepoint. (D–F) Differentially expressed miRNAs that are inversely regulated by GR24 and IBA treatments for the timepoints of 1 (D), 3 (E), or 7 (F) days after rooting. (G) Gene Ontology (GO) analysis for all identified target mRNAs by degradome sequencing. The highly enriched categories are shown as molecular function (MF, blue), cellular component (CC, orange), and biological process (BP, yellow). (H) Network representing the relationships between differentially expressed miRNAs and their target genes during AR formation. Blue ellipses represent the known miRNAs and green ellipses represent the novel miRNAs; yellow hexagons represent the target genes.

Figure 6. Correlative network analysis and degradome validation for the identified differentially expressed miRNAs and their target genes. (A–B) Correlative analysis for the identified differentially expressed miRNAs and their target genes from the comparison between the untreated controls and those treated with 10 μM GR24, 1 day (A) or 3 days (B) after rooting. The triangles represent miRNAs, and a larger triangle means that more target genes correlated with this miRNA. The curved lines represent target mRNAs: red represents a positive correlation and green represents a negative correlation. (C–E) Degradome sequencing validation for mdm-miR164a–*MdORE1* (C), mdm-miR164b–*MdORE1* (D), and mdm-miR397–*MdLAC3* (E) pairs. The heat map shows the expression profiles of miRNAs and their target genes. The secondary structure of the pre-miRNAs was predicted by the online software RNAfold. The blue arrows highlight the cleavage nucleotide positions on the target genes.

Figure 7. Target validation of mdm-miR164a/b-*MdORE1* module and phenotypic analysis of transgenic materials. (A-F) LUC activity assays of miRNAs degradation capability. (A) The cleavage sites of mdm-miR164a/b in *MdORE1* genetic structure. (B) Schematic diagrams of effector and reporter constructs. The precursors of mdm-miR164a and mdm-miR164b were fused into the effector vector and fragments including the predicted cleavage site of the predicted target genes were cloned into the reporter vector. The leaves of *Nicotiana benthamiana* were used to carry the dual-luciferase sensor system and the targeted degradation capability of miRNAs were visualized by LUC activities (C, D), the scale bar represents the luminescence intensity,

the red color indicates higher LUC activities while purple indicates lower LUC activities. The quantification of the luminescence intensities was calculated by LUC/REN (E and F), LUC: Luciferase activities; REN: Ranilla luciferase activities. (G-K) AR observation and quantity statistics of mdm-miR164b transgenic and wild materials. Values represent the mean ± SE of three biological replicates. Asterisks represent significant differences between each comparison using a two-tailed Student's t-test (** for P ⩽ 0.01).

Figure 8. *MdORE1* is involved in AR formation. (A) Phylogenetic analysis showed the evolutionary relationship of *MdORE1*(MD06G1196100) with *AtORE1*. (B) Subcellular localization of *MdORE1* in *N. benthamiana* leaves. GFP driven by 35S promotor was used as negative control. GFP signaling is indicated in green. Scale bars = 20 μm. (C) Schematic diagrams of VIGS construction. A specific fragment of *MdORE1* sequence (419 bp in length) was amplified from apple genome to construct the vector pTRV2-*MdORE1*. TRV strain ppk20 RNA2 driven by 35S promotor was regarded as a control. (D-G) Effects of silencing of *MdORE1* on the AR numbers and rooting rate in apple. Values represent the mean ± SE of three biological replicates. Asterisks represent significant differences between each comparison using a two-tailed Student's t-test (** for P ≤ 0.01).

Figure S1. Pairwise comparisons among different treatments for different timepoints. The bar plots show the number of DEGs for each comparison. Red represents upregulation, and green represents downregulation.

Figure S2. The enrichment of MapMan functional categories for the DEGs of pairwise comparisons. The heat map shows the level of enrichment in each category of DEGs. The significance of enrichment (*P*-value) is indicated by different colors.

Figure S3. Analysis of endogenous hormone levels. (A–F) Endogenous levels of IAA (A), GA4 (B), ABA (C), trans-Zeatin (D), ACC (E) and SA (F) under no treatment or GR24 treatment for all four timepoints. Values represent the mean ± SE of three biological replicates. Asterisks represent significant differences between the levels without treatment and with GR24 treatment at the same time point using a two-tailed Student's t-test (*for P ≤ 0.05 and **P ≤ 0.01).

Figure S4. SLs are involved in apple plant senescence regulation. Effects of GR24 treatment on apple leaves chlorophyll content (A), plant biomass and moisture content (H) during AR formation. GR24 concentration: 10 μM. Values represent the mean ± SE of three biological replicates. Asterisks represent significant differences between each comparison using a two-tailed Student's t-test (* for P ≤ 0.05; ** for P ≤ 0.01).

Figure S5. Length distribution of the unique small RNA reads from the high-throughput

small RNA sequencing data.

Figure S6. Summary of the distribution of six identified groups of miRNAs. The miRNA counts represent the number of miRNAs within each group. Expression level: middle indicates that the number of miRNA is more than 10 in at least one sample but less than the mean of all samples; high indicates that the number of miRNAs is greater than the mean in at least one sample.

Figure S7. Distribution of identified known miRNA in the 54 reported miRNA families.

Figure S8. Expression of identified negatively correlated miRNA–mRNA pairs at different timepoints. The heatmap on the left shows the miRNA expression level and that on the right shows the expression of the corresponding target genes.

Figure S9. LUC activity assays of *mdm-miRNA397* degradation capability. Values represent the mean ± SE of three biological replicates. Asterisks represent significant differences between each comparison using a two-tailed Student's t-test (** for $P \leq 0.01$).

Figure S10. The transcriptional level of ethylene synthesis gene *ACS4-like*(A) and signaling gene *EIN3*(B). Asterisks represent significant differences between each comparison using a two-tailed Student's t-test (** for $P \leq 0.01$).

Table S1. Summary of transcriptome data generated for all 30 samples.

Table S2. The DEGs inversely regulated between GR24- and IBA- treated groups.

Table S3. Known and novel miRNAs identified by small RNA sequencing.

Table S4. Degradome verified miRNA and their targets.

Table S5. Primer information used in this study.

Table 1 The small RNA sequencing data generated for 30 samples using Illumina sequencing platform.

	Raw reads (million)	Unique reads	mRNA	Repeats reads	Pfam reads					miRNA
					rRNA	Trna	snoRNA	snRNA	other Rfam RNA	
CK1	10.93	3048881	43302	217	7173	1115	475	226	643	2262759
CK2	16.49	5016490	61818	194	8270	1159	456	283	653	4001984
CK3	13.34	2839285	44698	242	9031	1345	544	293	723	2941443
1M1	11.04	2619832	29828	217	9359	1156	529	287	821	2158495
1M2	10.16	3432693	26108	203	9459	1122	459	273	816	1957106
1M3	13.55	3308373	40204	214	10069	1235	546	318	820	2589809
1G1	15.30	2294695	39109	225	12547	1540	638	409	960	2355494
1G2	11.47	2103847	26865	181	11629	1501	584	302	909	1614855
1G3	10.62	1907304	23304	178	10603	1306	564	300	865	1457036
1A1	11.87	1976103	16143	209	14545	2163	607	396	1050	1158140
1A2	12.47	1809315	16271	247	14650	2343	590	389	1094	1109301
1A3	11.58	2935646	12462	267	14383	2320	568	359	1100	910647
3M1	12.38	2578176	20657	198	11484	1374	487	331	885	1870054
3M2	13.13	1942898	16275	221	12107	1775	604	418	934	1448983
3M3	10.14	2580717	16186	156	9976	1230	447	245	796	1140075
3G1	15.41	2771289	17178	255	13506	2022	673	420	1055	1380427
1G2	16.68	2725080	20050	265	14205	2193	738	501	1106	1625866
3G3	12.04	3327670	17564	162	11422	1542	524	350	882	1594536
3A1	10.65	3648600	28410	230	8583	1055	508	231	749	2325289
1A2	13.42	3358162	36187	273	11045	1601	677	392	937	2615863
3A3	11.02	1324099	26863	139	7702	828	358	189	639	2331807
7M1	10.83	1910862	18565	279	11824	1904	699	445	1026	649248
7M2	11.76	2379059	20808	258	13504	1933	671	437	1084	1204100
7M3	12.21	2672874	24713	203	12454	1673	602	391	976	1447459
7G1	12.88	2910441	30524	161	8910	1027	531	259	745	1756487
7G2	14.71	3060858	42175	305	12197	1906	733	460	1051	2154840
7G3	10.39	1640204	22886	171	9748	1135	433	224	821	2267549
7A1	10.48	1686590	14192	212	11581	1663	547	331	944	936767
7A2	13.04	1581570	15100	230	12822	2129	717	478	1060	955188
7A3	10.77	3723917	14277	209	11899	1750	551	367	948	953973
Total	370.78	79115530	782722	6521	336687	47045	17060	10304	27092	53175580

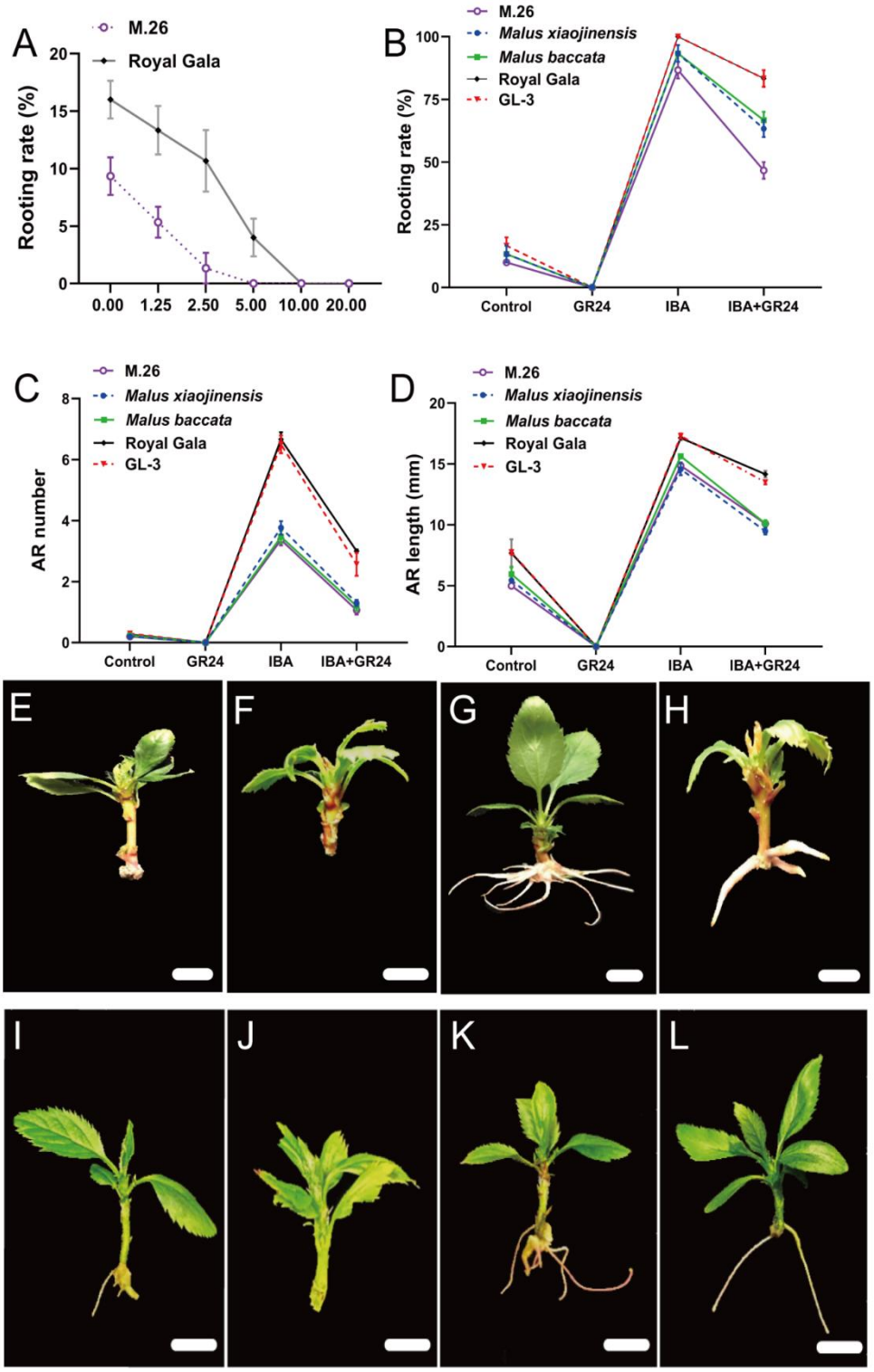
A
M.26
Royal Gala
Rooting rate (%)
0
5
10
15
20
0.00
1.25
2.50
5.00
10.00
20.00
B
M.26
Malus xiaojinensis
Malus baccata
Royal Gala
GL-3
Rooting rate (%)
0
25
50
75
100
Control
GR24
IBA
IBA+GR24
C
M.26
Malus xiaojinensis
Malus baccata
Royal Gala
GL-3
AR number
0
2
4
6
8
Control
GR24
IBA
IBA+GR24
D
M.26
Malus xiaojinensis
Malus baccata
Royal Gala
GL-3
AR length (mm)
0
5
10
15
20
Control
GR24
IBA
IBA+GR24
E
F
G
H
I
J
K
L

Figure 1. Adventitious root (AR) formation of *Malus* stem cuttings. (A) Complete inhibition of AR formation was observed at GR24 concentrations higher than 10 μM for M26 and Royal Gala. (B–D) Rooting efficiency (B), AR number (C), and AR length (D) of all five *Malus* materials either without treatment, or with 10 μM GR24 treatment, 0.3 mg L^{-1} IBA treatment or 10 μM GR24 + 0.3 mg L^{-1} IBA treatment. (E–H) Phenotype of M26 stem cuttings in control medium (E) or medium with 10 μM GR24 (F), 0.3 mg L^{-1} IBA (G) or 10 μM GR24 + 0.3 mg/L^{-1} IBA (H) for two weeks. (I–J). Phenotype of Royal Gala stem cuttings in control medium (I), or medium with 10 μM GR24 (J), 0.3 mg L^{-1} IBA (K) or 10 μM GR24 + 0.3 mg L^{-1} IBA (L) for two weeks. Bars represent 0.5 cm. The data for each time point are means for three biological replicates ± SE.

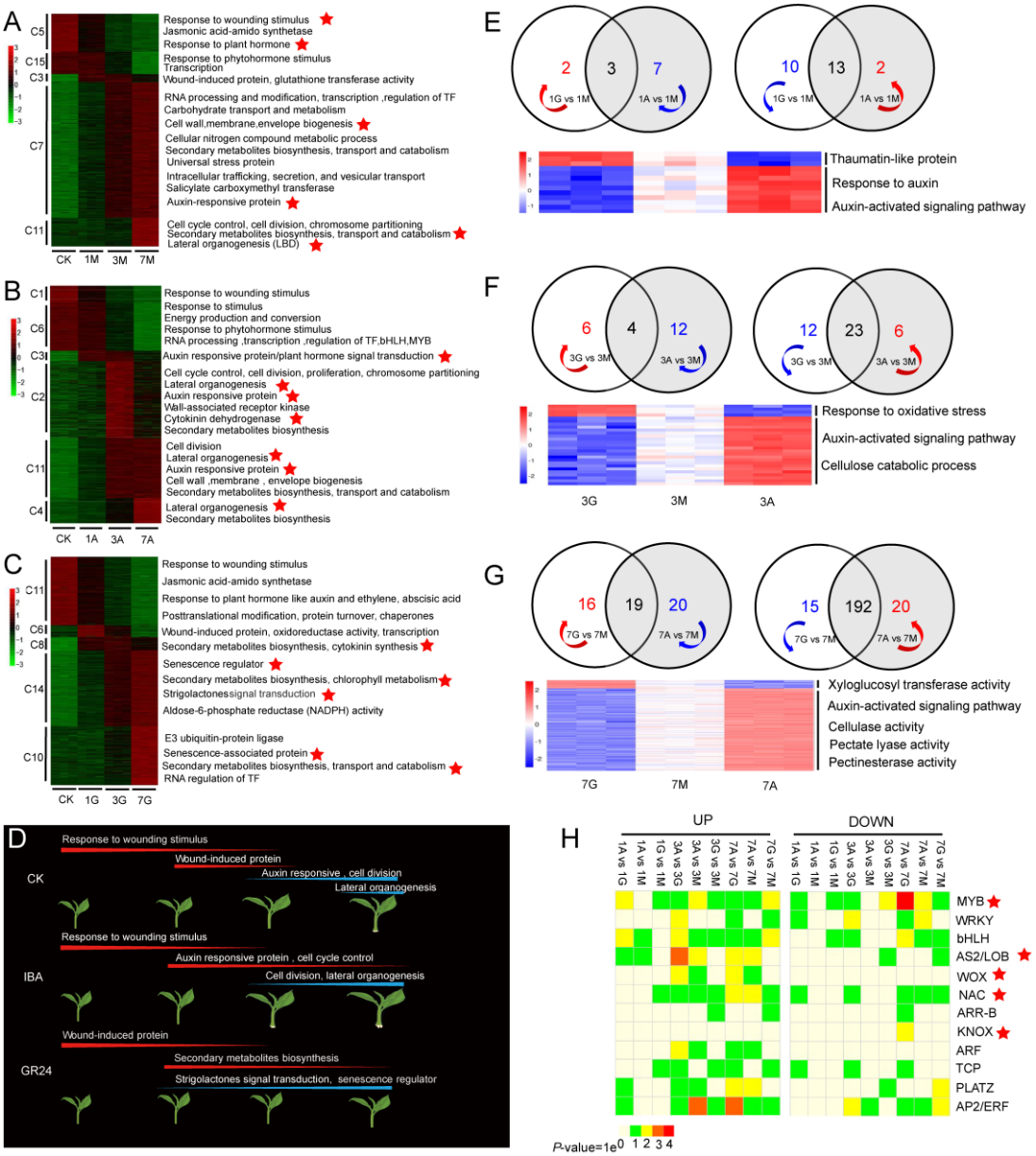
A
C5
C15
C3
C7
C11
Response to wounding stimulus
Jasmonic acid-amido synthetase
Response to plant hormone
Response to phytohormone stimulus
Transcription
Wound-induced protein, glutathione transferase activity
RNA processing and modification, transcription ,regulation of TF
Carbohydrate transport and metabolism
Cell wall,membrane,envelope biogenesis
Cellular nitrogen compound metabolic process
Secondary metabolites biosynthesis, transport and catabolism
Universal stress protein
Intracellular trafficking, secretion, and vesicular transport
Salicylate carboxymethyl transferase
Auxin-responsive protein
Cell cycle control, cell division, chromosome partitioning
Secondary metabolites biosynthesis, transport and catabolism
Lateral organogenesis (LBD)
CK 1M 3M 7M
B
C1
C6
C3
C2
C11
C4
Response to wounding stimulus
Response to stimulus
Energy production and conversion
Response to phytohormone stimulus
RNA processing ,transcription ,regulation of TF,bHLH,MYB
Auxin responsive protein/plant hormone signal transduction
Cell cycle control, cell division, proliferation, chromosome partitioning
Lateral organogenesis
Auxin responsive protein
Wall-associated receptor kinase
Cytokinin dehydrogenase
Secondary metabolites biosynthesis
Cell division
Lateral organogenesis
Auxin responsive protein
Cell wall ,membrane , envelope biogenesis
Secondary metabolites biosynthesis, transport and catabolism
Lateral organogenesis
Secondary metabolites biosynthesis
CK 1A 3A 7A
C
C11
C6
C8
C14
C10
Response to wounding stimulus
Jasmonic acid-amido synthetase
Response to plant hormone like auxin and ethylene, abscisic acid
Posttranslational modification, protein turnover, chaperones
Wound-induced protein, oxidoreductase activity, transcription
Secondary metabolites biosynthesis, cytokinin synthesis
Senescence regulator
Secondary metabolites biosynthesis, chlorophyll metabolism
Strigolactonessignal transduction
Aldose-6-phosphate reductase (NADPH) activity
E3 ubiquitin-protein ligase
Senescence-associated protein
Secondary metabolites biosynthesis, transport and catabolism
RNA regulation of TF
CK 1G 3G 7G
D
CK
Response to wounding stimulus
Wound-induced protein
Auxin responsive , cell division
Lateral organogenesis
IBA
Response to wounding stimulus
Auxin responsive protein , cell cycle control
Cell division, lateral organogenesis
GR24
Wound-induced protein
Secondary metabolites biosynthesis
Strigolactones signal transduction, senescence regulator
E
2
3
7
1G vs 1M
1A vs 1M
10
13
2
1G vs 1M
1A vs 1M
Thaumatin-like protein
Response to auxin
Auxin-activated signaling pathway
F
6
4
12
3G vs 3M
3A vs 3M
12
23
6
3G vs 3M
3A vs 3M
Response to oxidative stress
Auxin-activated signaling pathway
Cellulose catabolic process
3G 3M 3A
G
16
19
20
7G vs 7M
7A vs 7M
15
192
20
7G vs 7M
7A vs 7M
Xyloglucosyl transferase activity
Auxin-activated signaling pathway
Cellulase activity
Pectate lyase activity
Pectinesterase activity
7G 7M 7A
H
UP
DOWN
1A vs 1G
1A vs 1M
1G vs 1M
3A vs 3G
3A vs 3M
3G vs 3M
7A vs 7G
7A vs 7M
7G vs 7M
MYB
WRKY
bHLH
AS2/LOB
WOX
NAC
ARR-B
KNOX
ARF
TCP
PLATZ
AP2/ERF
P-value=1e0 1 2 3 4

Figure 2. Gene expression profiles and functional clustering over the time-course of AR formation under different treatments. (A–C) Heatmaps showing the gene expression profiles in k-means clusters without treatment (A), with IBA treatment (B) or with GR24 treatment (C). Red indicates higher expression, and green indicates low expression. (D) A schematic diagram of gene functional changes during AR formation under different treatments. The red lines show genes with reduced expression levels during AR formation and blue lines show genes with enhanced expression levels. (E–G) Identification of DEGs inversely regulated between GR24- and IBA-treated groups at 1 day (E), 3 days (F), or 7 days (G) after rooting. The overlapping region of the Venn diagrams represents DEGs that have the opposite expression pattern in IBA and GR24 treatments. The heatmap shows the expression level of each DEG in the overlapping region. (H) MapMan enrichment for transcription factor (TF) genes identified from the DEGs. The heatmap shows the level of enrichment for each category of TF. M: control; G: 10μM GR24-treatment; A: 0.3 mg L^{-1} IBA treatment.

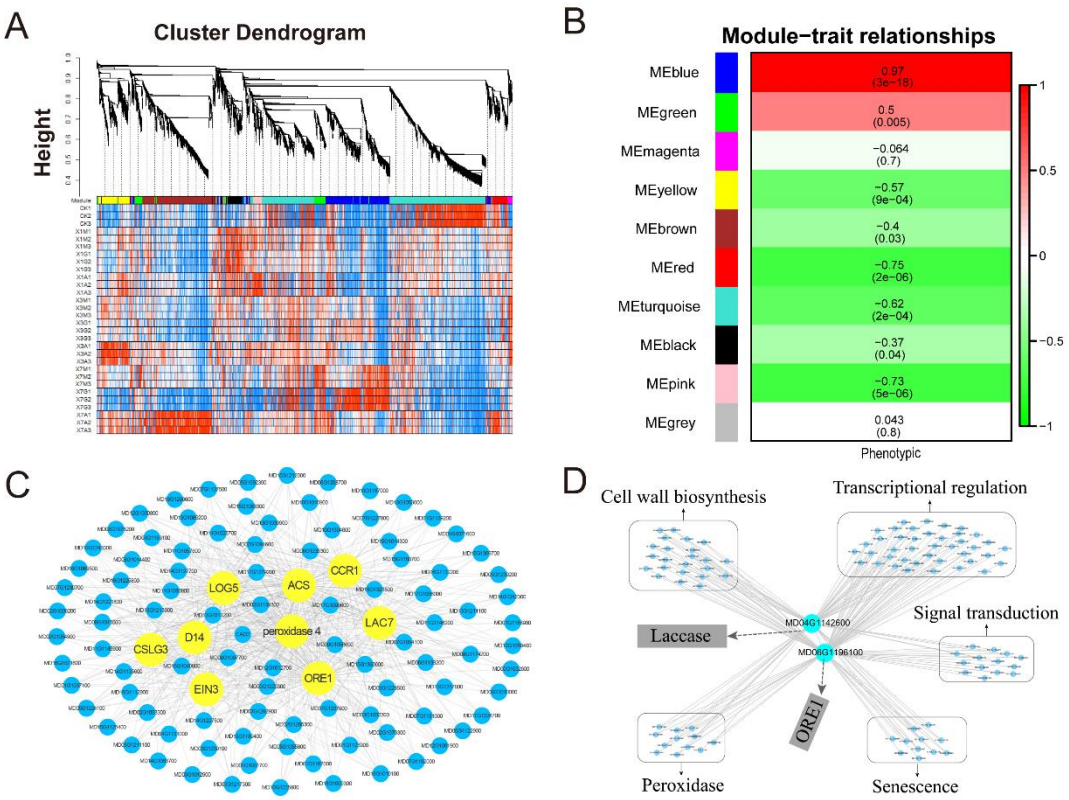
A
Cluster Dendrogram
Height
B
Module−trait relationships
MEblue
MEgreen
MEmagenta
MEyellow
MEbrown
MEred
MEturquoise
MEblack
MEpink
MEgrey
0.97
(3e−18)
0.5
(0.005)
−0.064
(0.7)
−0.57
(9e−04)
−0.4
(0.03)
−0.75
(2e−06)
−0.62
(2e−04)
−0.37
(0.04)
−0.73
(5e−06)
0.043
(0.8)
Phenotypic
1
0.5
0
−0.5
−1
C
LOG5
ACS
CCR1
LAC7
peroxidase 4
D14
CSLG3
EIN3
ORE1
D
Cell wall biosynthesis
Transcriptional regulation
Signal transduction
Laccase
MD04G1142600
MD08G1196100
ORE1
Peroxidase
Senescence

Figure 3. Co-expression network analysis of DEGs involved in AR formation. (A) Clustering dendrogram based on the dissimilarity topological overlap of genes across all samples. (B) Relationship between each module and each selected trait. The correlation value for each module–trait pair is shown from −1 (green) to 1 (red). The *P*-value for each module-trait comparison is displayed in parentheses. (C) In the blue module, nine co-expressed genes with a high node connectivity were identified (yellow circle). (D) Two hub genes (*MdLaccase* and *MdORE1*) were identified from a sub-network with 102 functional genes in the blue module.

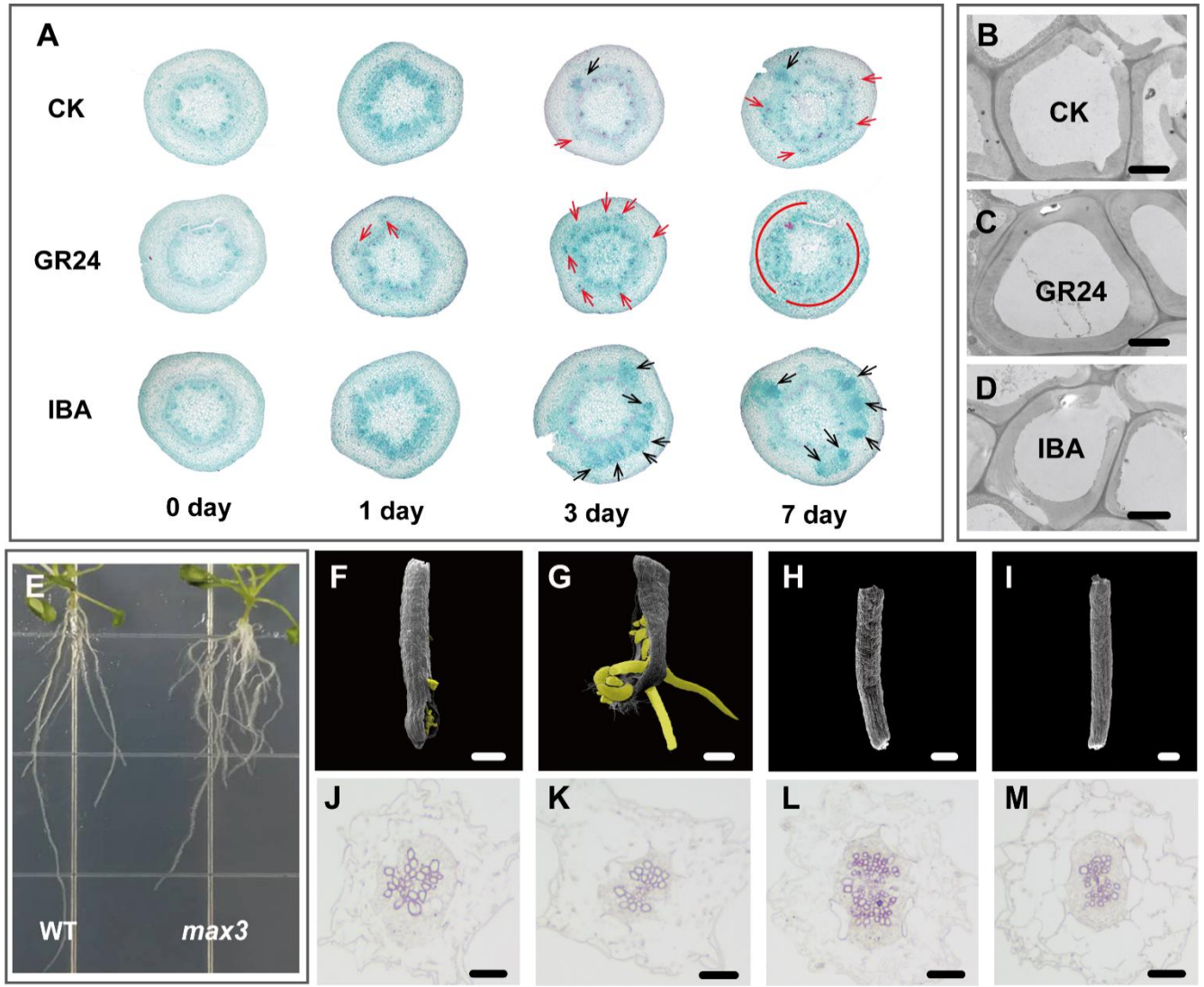
A
CK
GR24
IBA
0 day
1 day
3 day
7 day
B
CK
C
GR24
D
IBA
E
WT
max3
F
G
H
I
J
K
L
M

Figure 4. Anatomical observations of AR formation in apple stem cuttings. (A) Paraffin-embedded sections of apple stem cuttings without treatment, or with 10 μM GR24 treatment or 0.3 mg L^{-1} IBA treatment at all four timepoints. Black arrows represent root primordia and red arrows and lines represent enhanced cell wall growth. (B-D) Transmission electron micrographs of apple stem cuttings in the rooting medium without treatment (B), or with 10 μM GR24 (C) or 0.3 mg L^{-1} IBA treatment (D), bars = 0.5 μm. (E) Rooting ability of Arabidopsis WT and *max3* after 10 days in rooting medium. (F–I) Scanning electron micrographs of WT and *max3* mutant without treatment (F: WT; G: *max3*) or with 5 μM GR24 treatment (H: WT; I: *max3*) for 5 days. Yellow highlights represent ARs. Bars = 0.7 mm. (J–M) Histochemical staining with phloroglucinol-HCl for Arabidopsis WT and *max3* without treatment (J: WT; K: *max3*) or with 5 μM GR24 treatment (L: WT; M: *max3*) for 5 days. Bars = 0.1 mm.

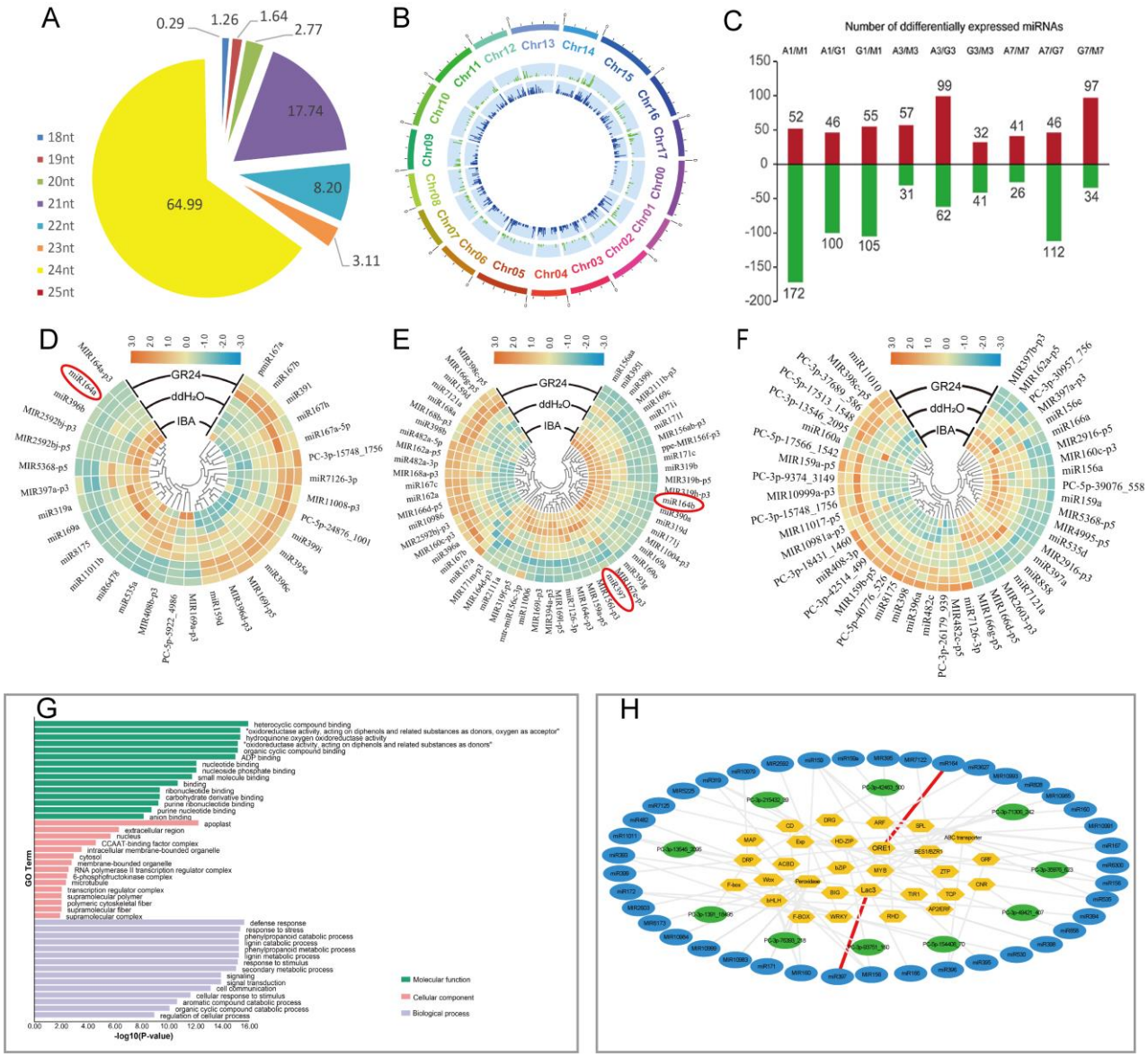
A
0.29
1.26
1.64
2.77
17.74
8.20
3.11
64.99
18nt
19nt
20nt
21nt
22nt
23nt
24nt
25nt
B
Chr01
Chr02
Chr03
Chr04
Chr05
Chr06
Chr07
Chr08
Chr09
Chr10
Chr11
Chr12
Chr13
Chr14
Chr15
Chr16
Chr17
Chr00
C
Number of ddifferentially expressed miRNAs
A1/M1
A1/G1
G1/M1
A3/M3
A3/G3
G3/M3
A7/M7
A7/G7
G7/M7
52
46
55
57
99
32
41
46
97
172
100
105
31
62
41
26
112
34
D
GR24
ddH₂O
IBA
E
GR24
ddH₂O
IBA
F
GR24
ddH₂O
IBA
G
heterocyclic compound binding
"oxidoreductase activity, acting on diphenols and related substances as donors, oxygen as acceptor"
hydroquinone:oxygen oxidoreductase activity
"oxidoreductase activity, acting on diphenols and related substances as donors"
organic cyclic compound binding
ADP binding
nucleotide binding
nucleoside phosphate binding
small molecule binding
binding
ribonucleotide binding
carbohydrate derivative binding
purine ribonucleotide binding
purine nucleotide binding
anion binding
apoplast
extracellular region
nucleus
CCAAT-binding factor complex
intracellular membrane-bounded organelle
cytosol
membrane-bounded organelle
RNA polymerase II transcription regulator complex
6-phosphofructokinase complex
microtubule
transcription regulator complex
supramolecular polymer
polymeric cytoskeletal fiber
supramolecular fiber
supramolecular complex
defense response
response to stress
phenylpropanoid catabolic process
lignin catabolic process
phenylpropanoid metabolic process
lignin metabolic process
response to stimulus
secondary metabolic process
signaling
signal transduction
cell communication
cellular response to stimulus
aromatic compound catabolic process
organic cyclic compound catabolic process
regulation of cellular process
GO Term
-log10(P-value)
Molecular function
Cellular component
Biological process
H

Figure 5. Sequencing analysis of small RNAs and the degradome. (A) A pie chart showing the length distribution of the identified small RNAs. (B) The circles show the distribution of known and novel small RNAs in the apple genome. The outermost circle represents the different chromosomes in the apple genome. From outer to inner, the circles represent known miRNAs (green) and novel miRNAs (blue). (C) Bar plot showing the number of DEGs for pairwise comparisons within each timepoint. (D–F) Differentially expressed miRNAs that are inversely regulated by GR24 and IBA treatments for the timepoints of 1 (D), 3 (E), or 7 (F) days after rooting. (G) Gene Ontology (GO) analysis for all identified target mRNAs by degradome sequencing. The highly enriched categories are shown as molecular function (MF, blue), cellular component (CC, orange), and biological process (BP, yellow). (H) Network representing the relationships between differentially expressed miRNAs and their target genes during AR formation. Blue ellipses represent the known miRNAs and green ellipses represent the novel miRNAs; yellow hexagons represent the target genes.

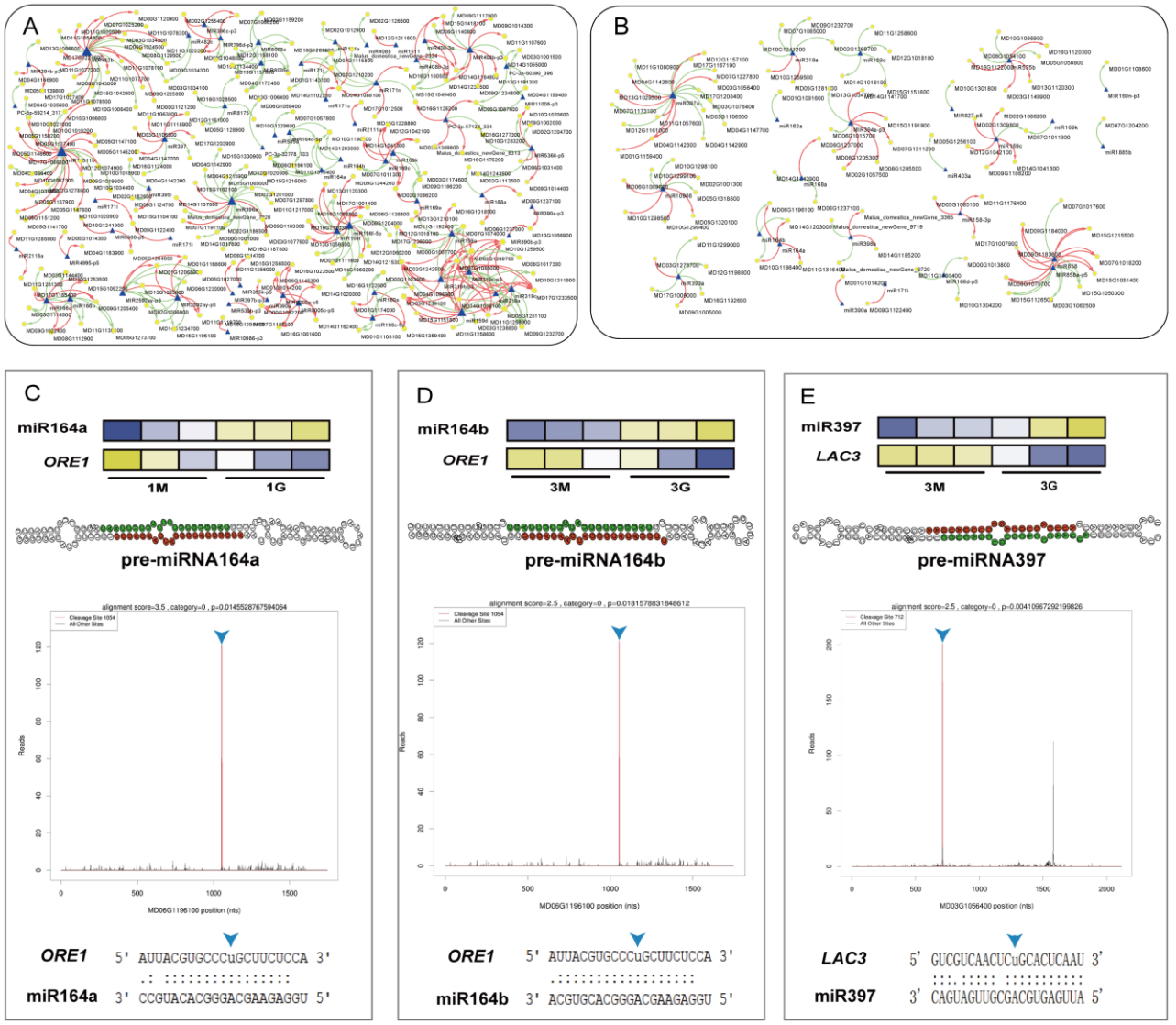
A
B
C
miR164a
ORE1
1M
1G
pre-miRNA164a
alignment score=3.5 , category=0 , p=0.014552876759406 4
Cleavage Site 1054
All Other Sites
Reads
MD06G1196100 position (nts)
ORE1 5' AUUACGUGCCCuGCUUCUCCA 3'
miR164a 3' CCGUACACGGGACGAAGAGGU 5'
D
miR164b
ORE1
3M
3G
pre-miRNA164b
alignment score=2.5 , category=0 , p=0.0191578831848612
Cleavage Site 1054
All Other Sites
Reads
MD06G1196100 position (nts)
ORE1 5' AUUACGUGCCCuGCUUCUCCA 3'
miR164b 3' ACGUGCACGGGACGAAGAGGU 5'
E
miR397
LAC3
3M
3G
pre-miRNA397
alignment score=2.5 , category=0 , p=0.00410967292199826
Cleavage Site 712
All Other Sites
Reads
MD03G1056400 position (nts)
LAC3 5' GUCGUCAACUCuGCACUCAAU 3'
miR397 3' CAGUAGUUGCGACGUGAGUUA 5'

Figure 6. Correlative network analysis and degradome validation for the identified differentially expressed miRNAs and their target genes. (A–B) Correlative analysis for the identified differentially expressed miRNAs and their target genes from the comparison between the untreated controls and those treated with 10 μM GR24, 1 day (A) or 3 days (B) after rooting. The triangles represent miRNAs, and a larger triangle means that more target genes correlated with this miRNA. The curved lines represent target mRNAs: red represents a positive correlation and green represents a negative correlation. (C–E) Degradome sequencing validation for mdm-miR164a–*ORE1* (C), mdm-miR164b–*ORE1* (D), and mdm-miR397–*LAC3* (E) pairs. The heat map shows the expression profiles of miRNAs and their target genes. The secondary structure of the pre-miRNAs was predicted by the online software RNAfold. The blue arrows highlight the cleavage nucleotide positions on the target genes.

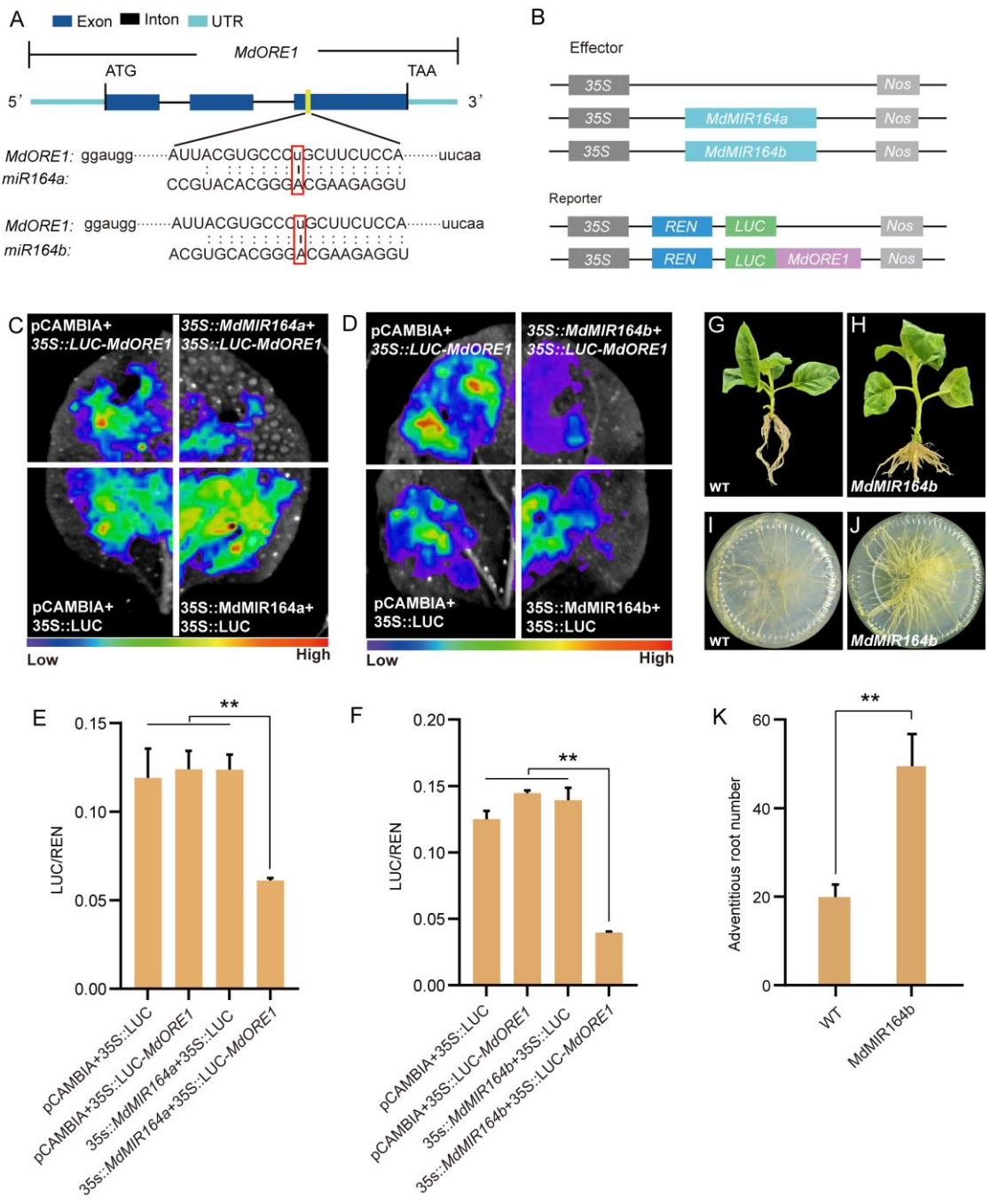
A
Exon
Inton
UTR
MdORE1
ATG
TAA
5'
3'
MdORE1: ggaugg AUUACGUGCCCUGCUUCUCCA uucaa
miR164a: CCGUACACGGGACGAAGAGGU
MdORE1: ggaugg AUUACGUGCCCUGCUUCUCCA uucaa
miR164b: ACGUGCACGGGACGAAGAGGU
B
Effector
35S
Nos
MdMIR164a
MdMIR164b
Reporter
REN
LUC
MdORE1
C
pCAMBIA+ 35S::LUC-MdORE1
35S::MdMIR164a+ 35S::LUC-MdORE1
pCAMBIA+ 35S::LUC
35S::MdMIR164a+ 35S::LUC
Low
High
D
pCAMBIA+ 35S::LUC-MdORE1
35S::MdMIR164b+ 35S::LUC-MdORE1
pCAMBIA+ 35S::LUC
35S::MdMIR164b+ 35S::LUC
Low
High
G
WT
H
MdMIR164b
I
WT
J
MdMIR164b
E
LUC/REN
0.15
0.10
0.05
0.00
**
pCAMBIA+35S::LUC
pCAMBIA+35S::LUC-MdORE1
35s::MdMIR164a+35S::LUC
35s::MdMIR164a+35S::LUC-MdORE1
F
LUC/REN
0.20
0.15
0.10
0.05
0.00
**
pCAMBIA+35S::LUC
pCAMBIA+35S::LUC-MdORE1
35s::MdMIR164b+35S::LUC
35s::MdMIR164b+35S::LUC-MdORE1
K
Adventitious root number
60
40
20
0
**
WT
MdMIR164b

Figure 7. Target validation of mdm-miR164a/b-*MdORE1* module and phenotypic analysis of transgenic materials. (A-F) LUC activity assays of miRNAs degradation capability. (A) The cleavage sites of mdm-miR164a/b in *MdORE1* genetic structure. (B) Schematic diagrams of effector and reporter constructs. The precursors of mdm-miR164a and mdm-miR164b were fused into the effector vector and fragments including the predicted cleavage site of the predicted target genes were cloned into the reporter vector. The leaves of *Nicotiana benthamiana* were used to carry the dual-luciferase sensor system and the targeted degradation capability of miRNAs were visualized by LUC activities (C, D), the scale bar represents the luminescence intensity, the red color indicates higher LUC activities while purple indicates lower LUC activities. The quantification of the luminescence intensities was calculated by LUC/REN (E and F), LUC: Luciferase activities; REN: Ranilla luciferase activities. (G-K) AR observation and quantity statistics of mdm-miR164b transgenic and wild materials. Values represent the mean ± SE of three biological replicates. Asterisks represent significant differences between each comparison using a two-tailed Student's t-test (** for $P \leqslant 0.01$).

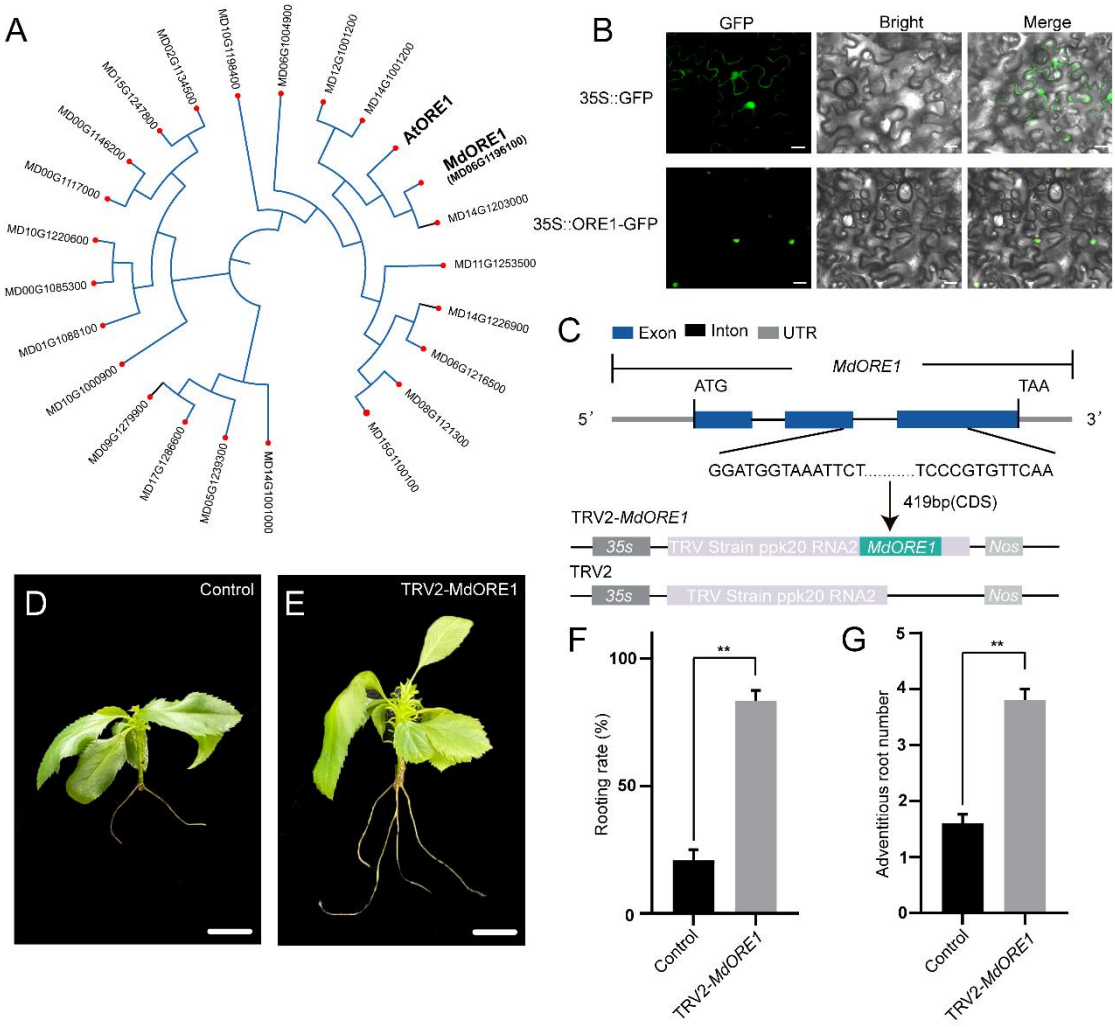
A
MD10G1199400
MD06G1004900
MD12G1001200
MD14G1001200
AtORE1
MdORE1
(MD06G1196100)
MD14G1203000
MD11G1253500
MD14G1226900
MD06G1216500
MD08G1121300
MD15G1100100
MD14G1001000
MD05G1239300
MD17G1286600
MD08G1279900
MD10G1000900
MD01G1088100
MD00G1085300
MD10G1220600
MD00G1117000
MD00G1146200
MD15G1247800
MD02G1134600
B
GFP
Bright
Merge
35S::GFP
35S::ORE1-GFP
C
Exon
Inton
UTR
MdORE1
ATG
TAA
5'
3'
GGATGGTAAATTCT.....TCCCGTGTTCAA
419bp(CDS)
TRV2-MdORE1
35s
TRV Strain ppk20 RNA2
MdORE1
Nos
TRV2
35s
TRV Strain ppk20 RNA2
Nos
D
Control
E
TRV2-MdORE1
F
Rooting rate (%)
100
50
0
**
Control
TRV2-MdORE1
G
Adventitious root number
5
4
3
2
1
0
**
Control
TRV2-MdORE1

Figure 8. *MdORE1* is involved in AR formation. (A) Phylogenetic analysis showed the evolutionary relationship of *MdORE1*(MD06G1196100) with *AtORE1*. (B) Subcellular localization of *MdORE1* in N. benthamiana leaves. GFP driven by 35S promotor was used as negative control. GFP signaling is indicated in green. Scale bars = 20 μm. (C) Schematic diagrams of VIGS construction. A specific fragment of *MdORE1* sequence (419 bp in length) was amplified from apple genome to construct the vector pTRV2-*MdORE1*. TRV strain ppk20 RNA2 driven by 35S promotor was regarded as a control. (D-G) Effects of silencing of *MdORE1* on the AR numbers and rooting rate in apple. Values represent the mean ± SE of three biological replicates. Asterisks represent significant differences between each comparison using a two-tailed Student's t-test (** for $P \leq 0.01$).

Figure S1. Pairwise comparisons among different treatments for different timepoints. The bar plots show the number of DEGs for each comparison. Red represents upregulation, and green represents downregulation.

Figure S2. The enrichment of MapMan functional categories for the DEGs of pairwise comparisons. The heat map shows the level of enrichment in each category of DEGs. The significance of enrichment (*P*-value) is indicated by different colors.

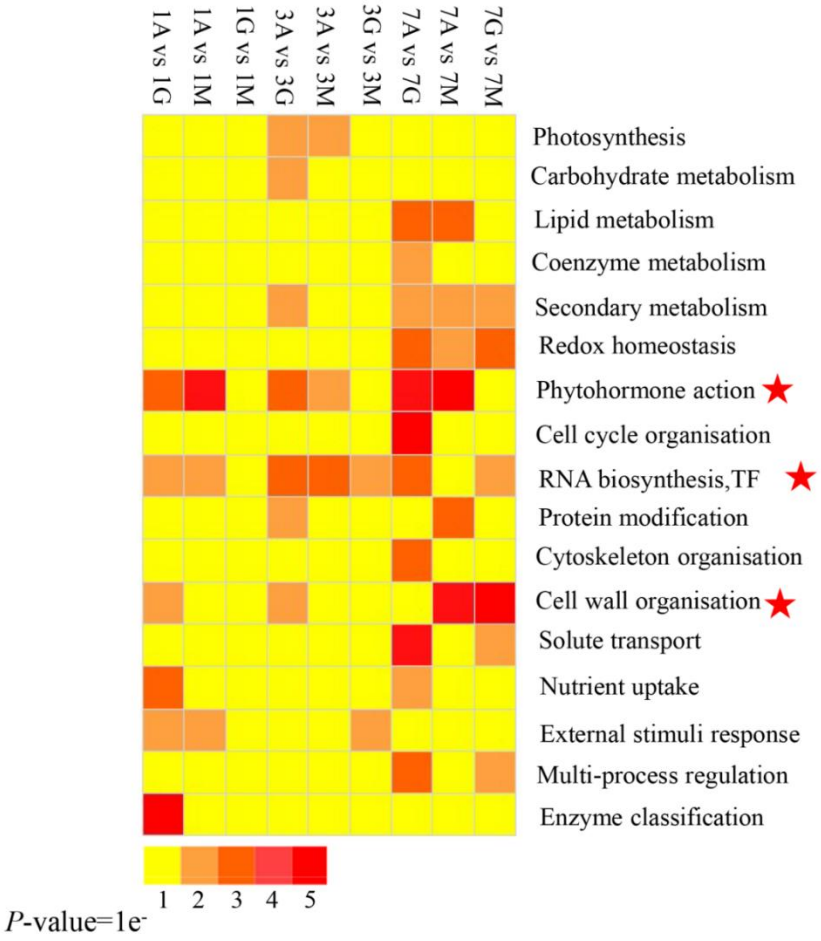

Figure S3. Analysis of endogenous hormone levels. (A–F) Endogenous levels of IAA (A), GA4 (B), ABA (C), trans-Zeatin (D), ACC (E) and SA (F) under no treatment or GR24 treatment for all four timepoints. Values represent the mean ± SE of three biological replicates. Asterisks represent significant differences between the levels without treatment and with GR24 treatment at the same time point using a two-tailed Student's t-test (*for $P \leq 0.05$ and **$P \leq 0.01$).

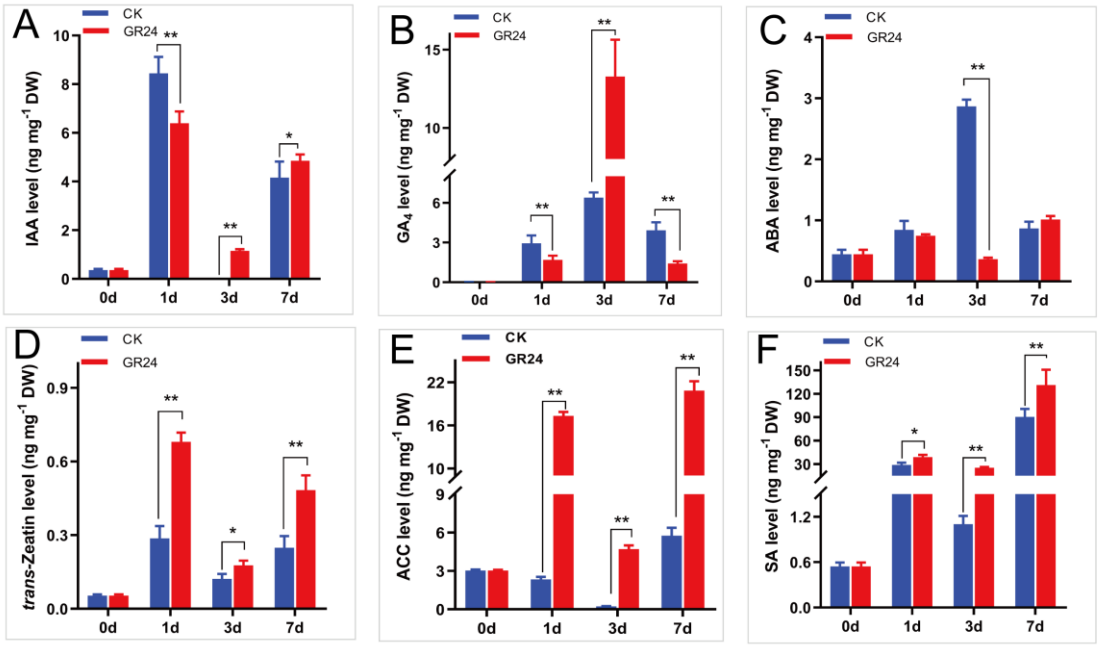

Figure S4. SLs are involved in apple plant senescence regulation. Effects of GR24 treatment on apple leaves chlorophyll content (A), plant biomass and moisture content (H) during AR formation. GR24 concentration: 10 μM. Values represent the mean ± SE of three biological replicates. Asterisks represent significant differences between each comparison using a two-tailed Student's t-test (* for $P \leq 0.05$; ** for $P \leq 0.01$).

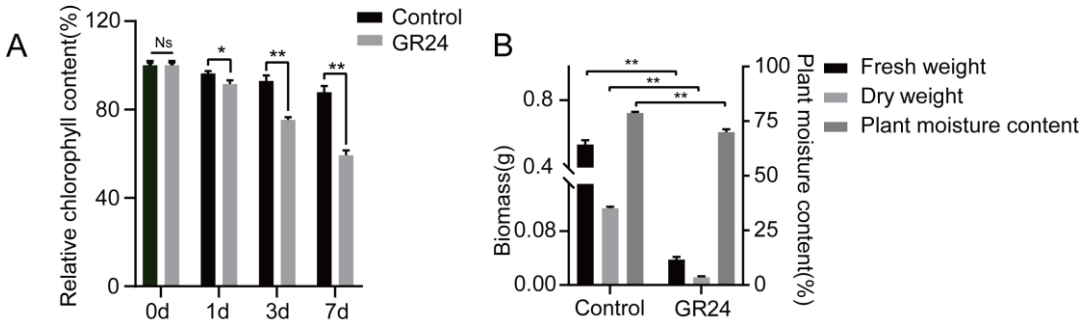

Figure S5. Length distribution of the unique small RNA reads from the high-throughput small RNA sequencing data.

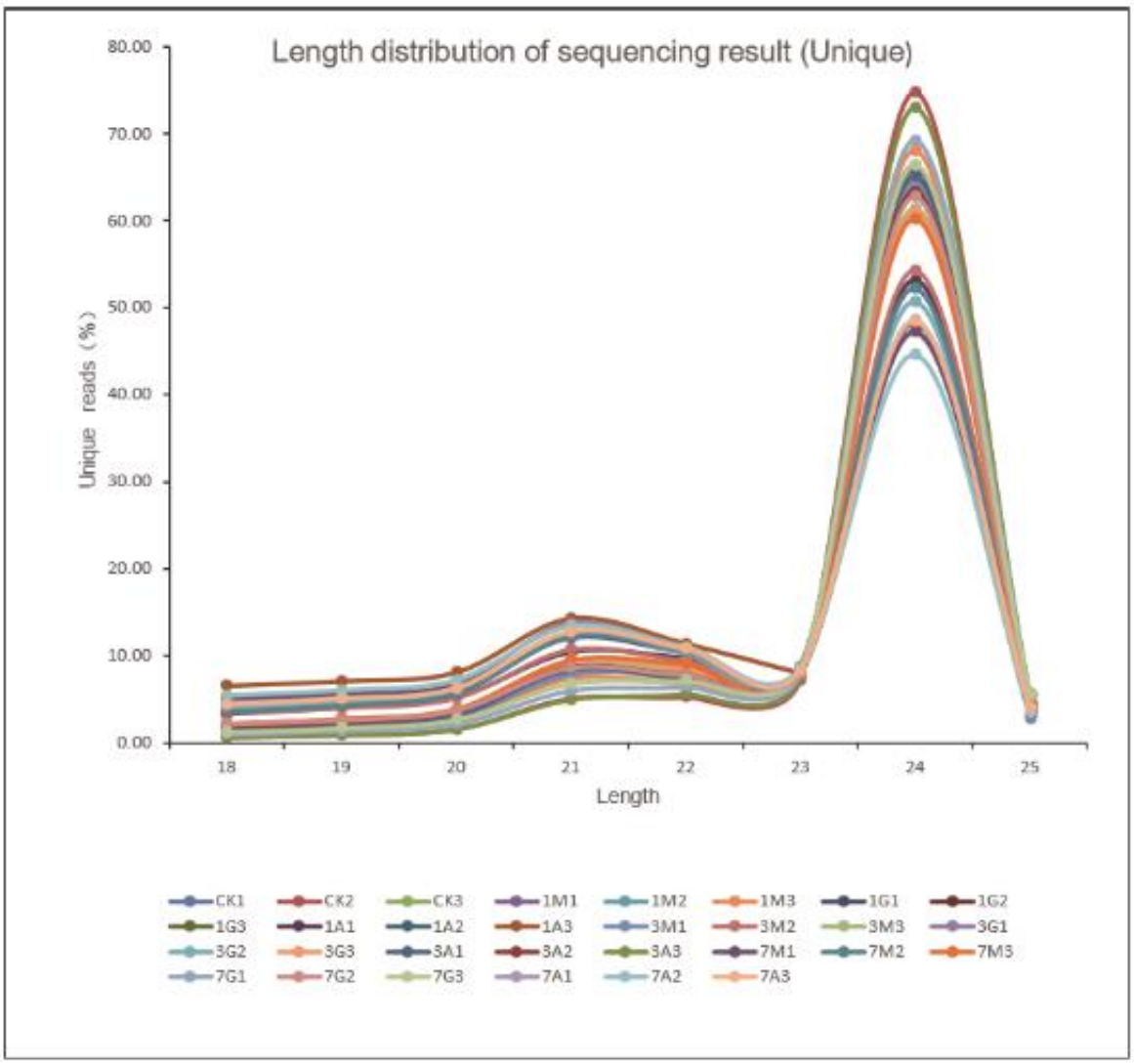

Figure S6. Summary of the distribution of six identified groups of miRNAs. The miRNA counts represent the number of miRNAs within each group. Expression level: middle indicates that the number of miRNA is more than 10 in at least one sample but less than the mean of all samples; high indicates that the number of miRNAs is greater than the mean in at least one sample.

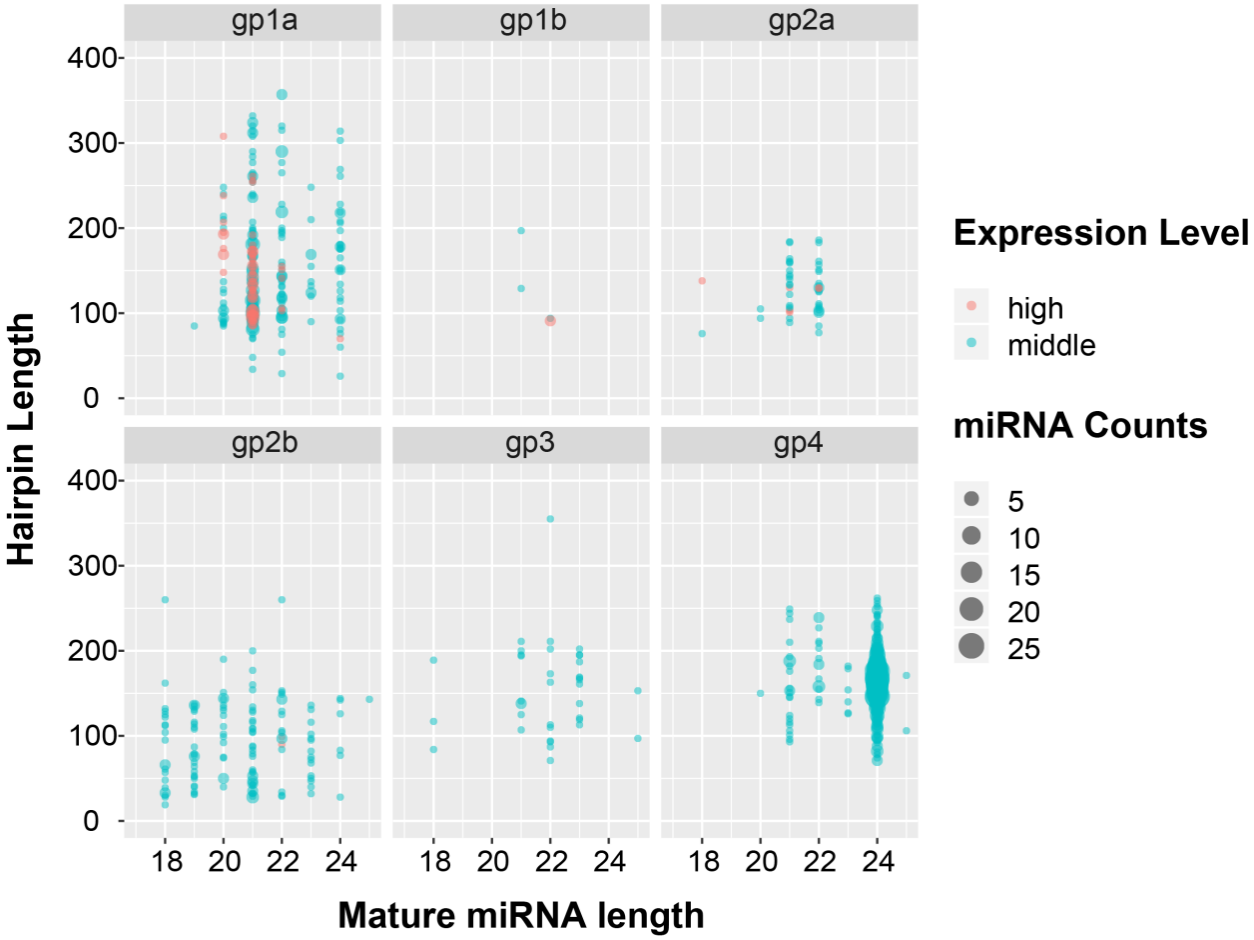

Figure S7. Distribution of identified known miRNA in the 54 reported miRNA families.

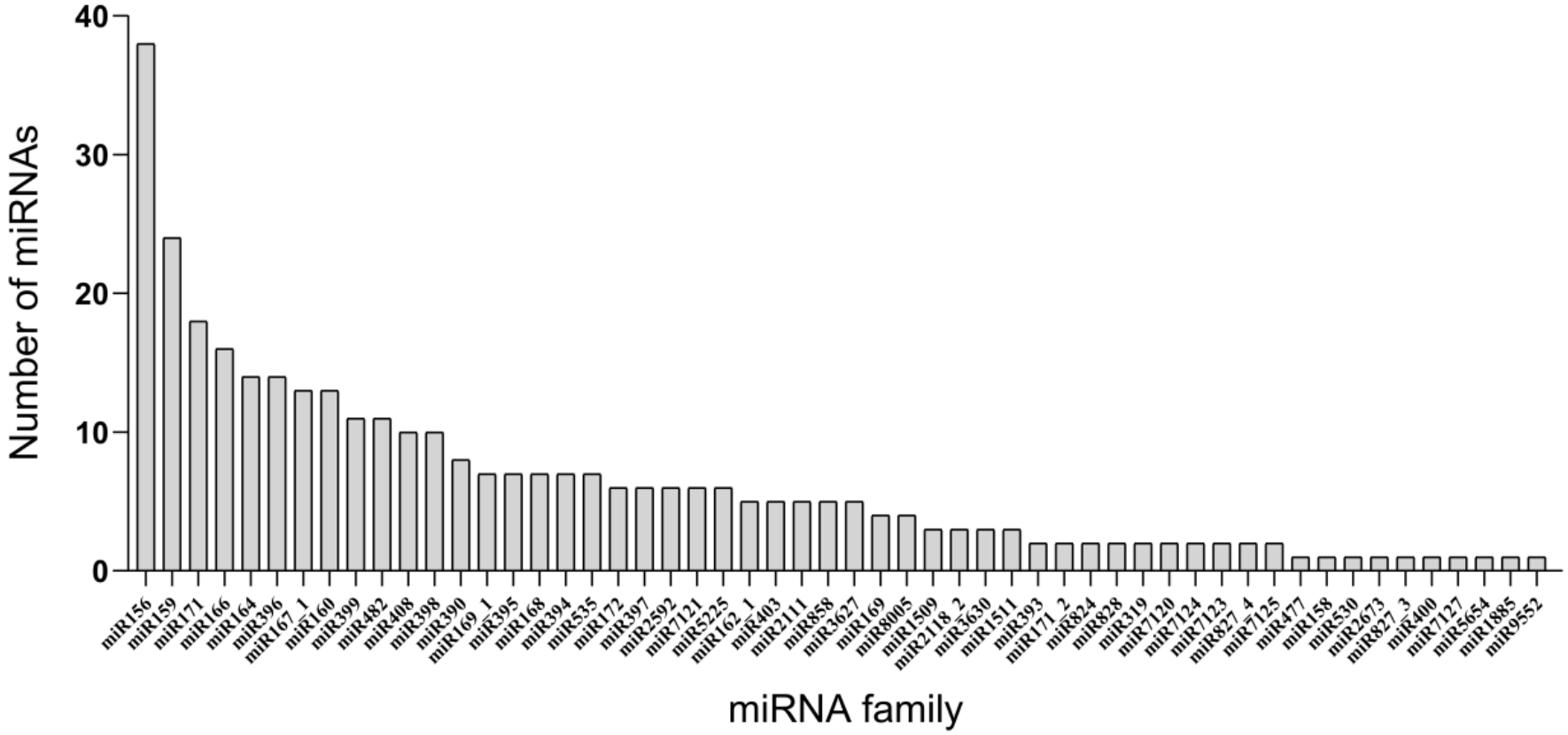

Figure S8. Expression of identified negatively correlated miRNA–mRNA pairs at different timepoints. The heatmap on the left shows the miRNA expression level and that on the right shows the expression of the corresponding target genes.

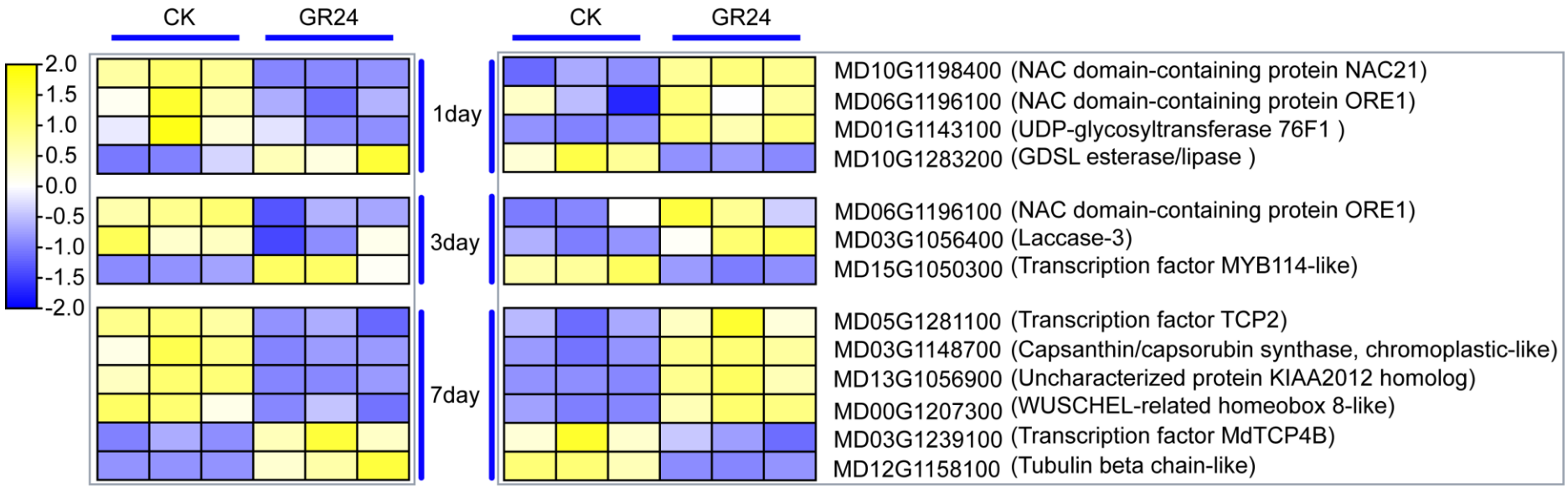

Figure S9. LUC activity assays of mdm-miRNA397 degradation capability. Values represent the mean ± SE of three biological replicates. Asterisks represent significant differences between each comparison using a two-tailed Student's t-test (** for P ≤ 0.01).

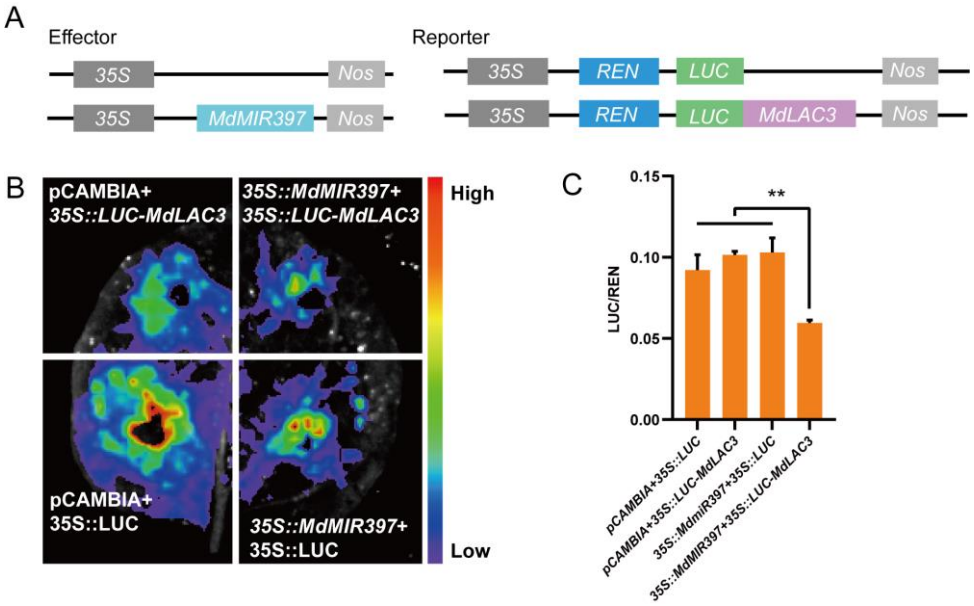

Figure S10. The transcriptional level of ethylene synthesis gene *ACS4-like* (A) and signaling gene *EIN3*(B). Asterisks represent significant differences between each comparison using a two-tailed Student's t-test (** for $P \leq 0.01$).

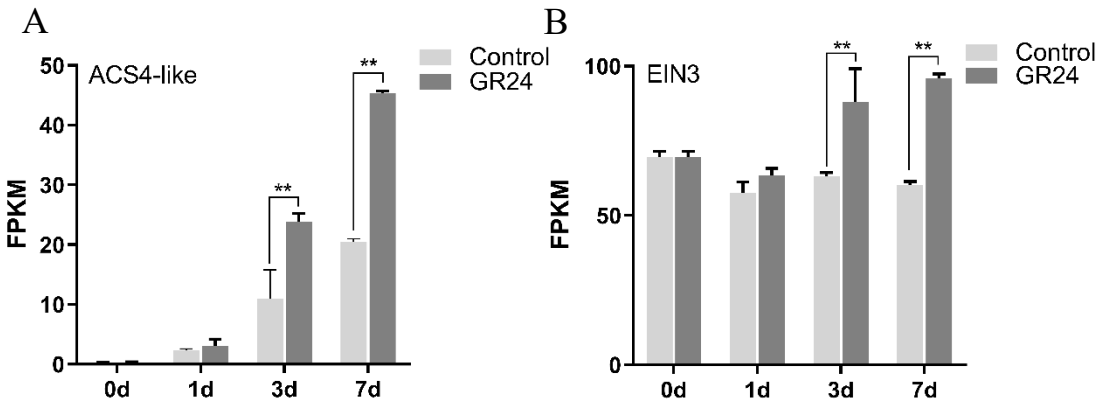

Table S1 Summary of transcriptome data generated for all 30 samples.

Samples	Clean Reads (million)	Mapped Reads (million)	Uniq Mapped Reads (million)	%≥Q30
CK1	69.42	64.85 (93.42%)	62.88 (90.59%)	92.27%
CK2	68.05	63.60 (93.46%)	61.68 (90.64%)	92.24%
CK3	51.74	48.42 (93.60%)	47.00 (90.87%)	92.29%
1A1	49.73	46.42 (93.33%)	44.98 (90.44%)	92.05%
1A2	58.90	55.10 (93.55%)	53.39 (90.64%)	92.20%
1A3	51.38	47.91 (93.24%)	46.47 (90.45%)	91.62%
1G1	51.57	48.15 (93.37%)	46.45 (90.07%)	92.01%
1G2	56.51	52.66 (93.18%)	50.98 (90.23%)	91.74%
1G3	51.99	48.68 (93.63%)	47.15 (90.69%)	92.45%
1M1	67.88	63.28 (93.22%)	60.87 (89.67%)	92.06%
1M2	52.70	49.19 (93.33%)	47.68 (90.47%)	91.62%
1M3	57.38	53.59 (93.39%)	51.79 (90.25%)	92.10%
3A1	48.52	45.36 (93.48%)	43.91 (90.50%)	92.30%
3A2	52.95	49.48 (93.45%)	47.97 (90.59%)	92.13%
3A3	50.33	46.99 (93.37%)	45.58 (90.57%)	92.07%
3G1	43.29	40.75 (94.13%)	39.25 (90.65%)	93.12%
3G2	49.05	46.14 (94.06%)	44.74 (91.21%)	93.15%
3G3	44.17	41.42 (93.76%)	40.17 (90.95%)	92.94%
3M1	52.13	48.58 (93.19%)	46.97 (90.10%)	91.75%
3M2	57.99	54.18 (93.42%)	52.52 (90.57%)	92.18%
3M3	42.67	39.83 (93.35%)	38.54 (90.33%)	92.06%
7A1	44.44	41.63 (93.67%)	40.29 (90.65%)	92.99%
7A2	44.97	42.20 (93.82%)	40.80 (90.72%)	93.49%
7A3	46.56	43.66 (93.76%)	42.30 (90.84%)	93.24%
7G1	55.20	51.52 (93.33%)	49.93 (90.44%)	92.39%
7G2	47.90	44.59 (93.09%)	43.26 (90.30%)	91.93%
7G3	45.68	42.66 (93.39%)	41.43 (90.69%)	92.37%
7M1	56.32	52.87 (93.87%)	51.29 (91.06%)	93.22%
7M2	46.70	43.81 (93.81%)	42.44 (90.88%)	93.35%
7M3	41.75	39.07 (93.59%)	37.80 (90.54%)	93.00%

TableS2-S4 were uploaded in separated files.

Table S5 Primers information used in this study

Names	Sequence
TRV2-MdORE1-F	ATTCTCTAGAAGGCCTCCATGGG
	GGATGGTAAATTCTCTGTCCACAAC
TRV2-MdORE1-R	ACGCGTGAGCTCGGTACCG
	TTGAACACGGGAACTGAAAATTCGG
MdORE1-F	GCCATGCGGTCATTACACTATCCCT
	GGATGGTAAATTCTCTGTCCACAAC
MdORE1-R	AGAATTCTGGCCAGCCTCTCCT
	TTGAACACGGGAACTGAAAATTCGG
MdLAC3-F	GCCATGCGGTCATTACACTATCCCT
	GCCGAAACGAGAAGTTCCCCT
MdLAC3-R	AGAATTCTGGCCAGCCTCTCCT
	TGTCGAAGGGCGCATTCTGGG